The Astrophysical Journal, 886:37 (19pp), 2019 November 20 https://doi.org/10.3847/1538-4357/ab35e6

Black Hole Spin and Accretion Disk Magnetic Field Strength Estimates for More Than 750 Active Galactic Nuclei and Multiple Galactic Black Holes

Ruth A. Daly[1,2]
[1] Penn State University, Berks Campus, Reading, PA 19608, USA; rdaly@psu.edu
[2] Center for Computational Astrophysics, Flatiron Institute, 162 5th Avenue, New York, NY 10010, USA
Received 2019 April 9; revised 2019 July 12; accepted 2019 July 12; published 2019 November 15

Abstract

Black hole systems, composed of a black hole, accretion disk, and collimated outflow, are studied here. Three active galactic nucleus (AGN) samples including 753 AGNs and 102 measurements of four stellar-mass galactic black holes (GBHs) are studied. Applying the theoretical considerations described by Daly, general expressions for the black hole spin function and accretion disk magnetic field strength are presented and applied to obtain the black hole spin function, spin, and accretion disk magnetic field strength in dimensionless and physical units for each source. Relatively high spin values are obtained; spin functions indicate typical spin values of about 0.6–1 for the sources. The distributions of accretion disk magnetic field strengths for the three AGN samples are quite broad and have mean values of about 10^4 G, while those for individual GBHs have mean values of about 10^8 G. Good agreement is found between spin values obtained here and published values obtained with well-established methods; comparisons for one GBH and six AGNs indicate that similar spin values are obtained with independent methods. Black hole spin and disk magnetic field strength demographics are obtained and indicate that black hole spin functions and spins are similar for all of the source types studied, including GBHs and different categories of AGNs. The method applied here does not depend on any specific accretion disk emission model and does not depend on a specific model that relates jet beam power to compact radio luminosity; hence, the results obtained here can be used to constrain and study these models.

Key words: accretion, accretion disks – black hole physics – galaxies: active – galaxies: jets

Supporting material: machine-readable tables

1. Introduction

Several methods have been proposed to measure and study the spin properties of supermassive black holes associated with active galactic nuclei (AGNs) and stellar-mass black holes referred to as galactic black holes (GBHs). These methods include the use of emission from the accretion disk associated with the black hole (Fabian et al. 1989; Miller et al. 2009; Patrick et al. 2012; Walton et al. 2013; Vasudevan et al. 2016; Reynolds 2019, and references therein), the use of the properties of extended radio sources (Daly 2009a, 2009b, 2011; Daly & Sprinkle 2014), a combination of accretion disk emission and the properties of radio sources (Gnedin et al. 2012; Daly 2016; Mikhailov & Gnedin 2018), and the properties of gravitational waves (Abbott et al. 2018). To date, studies of emission from the accretion disk alone have led to about 22 AGNs with "robust" spin determination based on the X-ray reflection method (e.g., Reynolds 2019 and references therein), and disk emission has led to several GBH spin determinations (e.g., Miller et al. 2009; King et al. 2013, and references therein). Studies of outflows from powerful extended radio sources have led to about 130 spin determinations (e.g., Daly & Sprinkle 2014), while studies that combine the disk emission and outflow properties provide a few hundred spin values (e.g., Gnedin et al. 2012; Daly 2016; Mikhailov & Gnedin 2018).

Here, accretion disk emission properties are combined with the properties of radio sources associated with the collimated outflow from a black hole to estimate black hole spin functions and spins for 753 AGNs and four GBHs using the method proposed by Daly (2016) and extended here. The "black hole system" includes the black hole, the accretion disk, and the collimated outflow. Background information on measuring black hole spin for sources with collimated outflows is provided in Section 1.1.

In addition to providing a black hole spin estimate, the method introduced by Daly (2016) and extended here allows an estimate of the magnetic field strength of the accretion disk of each source in a manner that does not depend on a detailed model of the accretion disk. Here and throughout the paper, the term "magnetic field strength" indicates the magnitude of the magnetic field, B, of the accretion disk.

1.1. Background on Black Hole Systems with Collimated Outflows

To empirically determine and study black hole spin, sources for which the spin is likely to affect some empirically accessible aspect of the source are selected for study. Black hole systems with powerful outflows, especially those with outflows that are powerful relative to the accretion disk bolometric luminosity, are likely to be powered at least in part by the spin of the black hole (e.g., Blandford & Znajek 1977; Begelman et al. 1984; Blandford 1990; Meier 1999, 2001; Yuan & Narayan 2014; Blandford et al. 2019). This is based on the premise that the spin energy of the black hole can be extracted (Penrose 1969; Penrose & Floyd 1971).

Thus, sources with powerful collimated outflows are considered here. The beam power, $L_j \equiv dE/dt$, is the energy per unit time ejected by the black hole system in the form of a collimated jet. The beam power is typically considered to be in the form of directed kinetic energy, and the jet manifests its presence as a compact or extended radio source. The beam powers of classical double radio sources discussed here were obtained with the "strong shock method," described in detail below.

A source with both a beam power and black hole mass determination can be used to solve for a combination of the black hole spin and accretion disk braking magnetic field strength (Daly 2009a, 2009b, 2011; Daly & Sprinkle 2014; Mikhailov & Gnedin 2018). For example, Daly (2011) and Daly & Sprinkle (2014) assumed three different parameterizations of the magnetic field strength and solved for black hole spin values given these field strengths. Thus, a second equation is needed to be able to break this magnetic field strength—black hole spin degeneracy and solve for the spin and accretion disk magnetic field strength separately.

To be able to break this degeneracy, Daly (2016, hereafter D16) considered sources that have bolometric accretion disk luminosity determinations in addition to values for the beam power and black hole mass. This led to a sample of 97 powerful classical double radio sources. This study indicated an empirically determined relationship between the beam power, accretion disk bolometric luminosity, $L_{\rm bol}$, and Eddington luminosity, $L_{\rm Edd}$, of the form

$$\frac{L_j}{L_{\rm bol}} \propto \left(\frac{L_{\rm bol}}{L_{\rm Edd}}\right)^{\alpha_*} \propto \left(\frac{L_{\rm bol}}{L_{\rm Edd}}\right)^{A-1}, \quad (1)$$

where the parameter α_* is related to the parameter A by $\alpha_* = (A-1)$; a best-fit value of $\alpha_* = -0.56 \pm 0.05$ was obtained. Equation (1) is referred to as the fundamental line (FL) of black hole activity. The Eddington luminosity is given by $L_{\rm Edd} \simeq 1.3 \times 10^{46} M_8\,{\rm erg\,s^{-1}}$, where M_8 is the black hole mass in units of $10^8\,M_\odot$. The 97 sources included in the study are powerful classical double radio sources, known as FR II sources (Fanaroff & Riley 1974).

The beam powers were determined using the "strong shock" method; the method is based on the application of the equations of strong shock physics (i.e., the strong shock jump conditions) to powerful classical double sources (Daly 1994). The method can only be applied to FR II radio sources with very regular radio bridge or lobe structure, which corresponds to sources with 178 MHz radio powers greater than about $8 \times 10^{27}\,{\rm W\,Hz^{-1}}$ for a value of Hubble's constant of $70\,{\rm km\,s^{-1}\,Mpc^{-1}}$ (Leahy & Williams 1984; Leahy et al. 1989; Wellman et al. 1997a, 1997b; O'Dea et al. 2009). The cigar-like lobe structure indicates that the sources are not self-similar, which is also indicated by detailed studies of the source shapes (e.g., Leahy & Williams 1984; Leahy et al. 1989; Wellman et al. 1997a; Daly et al. 2010). The method requires the use of high-resolution multifrequency radio maps covering the full radio lobe region of each source. O'Dea et al. (2009) showed that this method is essentially model independent: it has no free parameters and does *not* rely on whether the radio-emitting plasma is close to minimum energy or equipartition conditions when the magnetic field strength in the extended radio lobe is less than or equal to the minimum energy value (see Section 3.3 of O'Dea et al. 2009), which is consistent with measured offsets from minimum energy conditions in sources of this type (e.g., Wellman et al. 1997a, 1997b; Croston et al. 2004, 2005; Shelton et al. 2011; Godfrey & Shabala 2013; Harwood et al. 2016). When the beam power is written in terms of empirically determined strong shock parameters, the parameterized deviations of the relativistic electron population and magnetic field strength of the plasma in the extended radio source from minimum energy (or equipartition) conditions fortuitously cancel out. Beam powers for additional sources were obtained by applying the relationship between beam power obtained with the strong shock method and radio power (Daly et al. 2012). The beam powers obtained for the FR II sources discussed here using the strong shock method are thought to be very reliable. From a strictly empirical perspective, these beam powers are the foundation of the use of FR II sources for cosmological studies and are found to yield coordinate distances and first and second derivatives of the coordinate distance with respect to redshift that are in excellent agreement with those obtained using Type Ia supernovae from a redshift of about 0 to a redshift greater than 1 (e.g., Daly et al. 2008). The black hole masses were obtained from McLure et al. (2006, 2004) and Tadhunter et al. (2003). The bolometric accretion disk luminosities, $L_{\rm bol}$, were obtained from the [O III] luminosities using the relationship obtained by Heckman et al. (2004) and confirmed by Dicken et al. (2014). The [O III] luminosities were obtained from Grimes et al. (2004).

To understand the implications of the empirical relationship given by Equation (1), general theoretical expressions were considered. The beam power is parameterized as $L_j \propto \dot{m}^a\, M^b\, f(j)$, where M is the black hole mass, $f(j)$ is a function of the spin of the black hole, and the bolometric disk luminosity is parameterized as $L_{\rm bol} \propto \epsilon \dot{M} \propto \epsilon\, \dot{m}\, M$, where $\dot{M}$ is the mass accretion rate, $\dot{m} \equiv \dot{M}/\dot{M}_{\rm Edd}$ is the dimensionless mass accretion rate, $\dot{M}_{\rm Edd} \equiv L_{\rm Edd} c^{-2}$ is the Eddington accretion rate, and ϵ is a dimensionless efficiency factor. The efficiency ϵ and the dimensionless mass accretion rate $\dot{m}$ are each normalized to have a maximum value of unity. The spin function $f(j)$ is considered to be independent of the mass accretion rate and black hole mass. Here, the notation of Blandford (1990) and Meier (1999) is used; the dimensionless black hole spin j is defined in the usual way, $j \equiv Jc/(GM^2)$, where J is the spin angular momentum of the hole, M is the black hole mass, c is the speed of light, and G is Newton's constant; in other work, j is sometimes represented with the symbol a or a_*. The Meier (1999) model is a hybrid that includes a disk wind, as in the model of Blandford & Payne (1982), and black hole spin energy extraction, as in the model of Blandford & Znajek (1977). The normalizations are parameterized by g_j and $g_{\rm bol}$, where the maximum values of the beam power and bolometric luminosities are given by $L_j({\rm max}) = g_j L_{\rm Edd}$ and $L_{\rm bol}({\rm max}) = g_{\rm bol} L_{\rm Edd}$, respectively. This form for L_j is motivated by the form of the equation for the beam power in black-hole-spin-powered outflow models: $L_j \propto \dot{m}\, M\, f(j) \propto B_p^2\, M^2\, f(j)$, that is, $B_p^2 \propto (\dot{m}/M)$ (e.g., Blandford & Znajek 1977; Blandford 1990; Meier 1999; Tchekhovskoy et al. 2010; Yuan & Narayan 2014), where B_p is the poloidal component of the accretion disk magnetic field. A spin term is not included in the expression for $L_{\rm bol}$ because this is expected to be important only as $L_{\rm bol}/L_{\rm Edd} \rightarrow 1$, which would only impact a small fraction of the sources considered; as the sample sizes become larger, it will be possible to look for the signature of the impact of spin on $L_{\rm bol}$.

The theoretical expressions are applied to the empirical relationships to understand the implications of the results. Equation (1) indicates that $\dot{m}^a\, M^b\, f(j) \propto (\epsilon\, \dot{m})^A M$, which suggests that $b = 1$. In this case, the ratio of $L_j/L_{\rm bol}$ is expected to be independent of black hole mass, which is confirmed to be the case for the sample studied by D16. A value of $b = 1$ indicates that $\dot{m}^a\, M\, f(j) \propto (\epsilon\, \dot{m})^A M$, so $\dot{m}^a = (\epsilon\, \dot{m})^A$, since $f(j)$ is independent of $\dot{m}$ and M by construction, and ϵ and $\dot{m}$ are each normalized to have a maximum value of 1. While this general solution leads to Equation (2), it is interesting to pause

for a moment and consider the two simplest particular solutions for $A \simeq 1/2$ (obtained by D16): that obtained with $a = 1$, indicating $\epsilon \propto \dot{m}$, and that obtained for $a = 1/2$, indicating $\epsilon =$ constant. The first particular solution indicates $L_j \propto \dot{m}\, M\, f(j)$ with $L_{\rm bol} \propto \dot{m}^2\, M$. The second particular solution indicates $L_j \propto \dot{m}^{1/2}\, M\, f(j)$ with $L_{\rm bol} \propto \dot{m}\, M$. This means that the combination $L_j \propto \dot{m}\, M\, f(j)$ and $L_{\rm bol} \propto \dot{m}\, M$ is inconsistent with the empirical results obtained by D16.

The general solution obtained above indicates that (see Equations (4) and (5) of D16), independent of the value of a,

$$\frac{f(j)}{f_{\rm max}} = \left(\frac{L_j}{g_j L_{\rm Edd}}\right)\left(\frac{L_{\rm bol}}{g_{\rm bol} L_{\rm Edd}}\right)^{-A} . \quad (2)$$

The spin function $f(j)$ is normalized by its maximum value $f_{\rm max}$, which is the value of $f(j)$ when $j = 1$.

It will be shown in Section 3 that the same expression can be derived for other sources that fall on the FL of black hole activity. The spin function can be converted to black hole spin j, as discussed in Section 4. The quantity $\sqrt{(f(j)/f_{\rm max})} \propto j$ to first order in most outflow models, so this is the quantity obtained and studied here. In the Blandford–Znajek model (1977) and the Meier (1999) models, the conversion is $\sqrt{f(j)/f_{\rm max}} = j(1 + \sqrt{1 - j^2})^{-1}$, though numerical simulations suggest that this equation may be modified for some outflow models (e.g., Tchekhovskoy et al. 2010; Yuan & Narayan 2014).

Given the results reported by D16, it was interesting to consider whether the fundamental plane (FP) of black hole activity, which is written in terms of observed quantities, is the empirical manifestation of the same underlying relationship as that described by Equation (1). Daly et al. (2018, hereafter D18) showed that this is indeed the case.

There are many equivalent representations of the FP, which is a relationship that applies to sources with *compact* radio emission, disk X-ray emission, and an estimate of the black hole mass. The FP was introduced by Merloni et al. (2003, hereafter M03) and Falcke et al. (2004). Here, the representation presented by Nisbet & Best (2016, hereafter NB16) is followed; other representations can easily be obtained from this by making appropriate substitutions as described by NB16:

$$\log L_R = a \log L_{\rm X,42} + b \log M_8 + c , \quad (3)$$

where a, b, and c are empirically determined constants and may be different for different source samples (note that these are unrelated to the quantities a and b discussed earlier); L_R is the 1.4 GHz radio power of the compact radio source in erg s^{-1}; $L_{\rm X,42}$ is the (2–10) keV X-ray luminosity of the disk in units of 10^{42} erg s^{-1}; and M_8 is the black hole mass in units of $10^8\, M_\odot$; conversions to and from other wavebands are discussed by NB16. NB16 present results obtained with a sample of 576 LINERs and summarize results obtained by M03, Körding et al. (2006a, 2006b), Gültekin et al. (2009), Bonchi et al. (2013), and Saikia et al. (2015, hereafter S15).

For FP sources, D18 showed that, using standard, well-accepted equations relating the compact radio luminosity to the beam power and the disk X-ray luminosity to the bolometric disk luminosity, the FP can be written in the form of Equation (1) without specifying a value of α_* or A, and best-fit FP parameters can be used to obtain the beam power from the compact radio luminosity. Specifically, the beam power is written as

$$\log L_j = C \log L_R + D , \quad (4)$$

and the bolometric disk luminosity is written as

$$L_{\rm bol} = \kappa_{\rm X}\, L_{\rm X}(2\text{–}10\ {\rm keV}), \quad (5)$$

where C, D, and $\kappa_{\rm X}$ are constant for a given source sample and $L_{\rm X}$(2–10 keV) is the (2–10) keV luminosity of the source. Given Equations (4) and (5), D18 showed that Equation (3) can be written in the form of Equation (1). The results indicate that the value of C is related to the best-fit FP parameters a and b: $C = 1/(a+b)$; D depends on a series of empirically determined constants, including best-fit FP parameters a, b, and c, $\kappa_{\rm X}$, and a normalization factor, B, obtained using the strong shock method, as described in detail by D18.

Thus, the beam power L_j can be obtained empirically in a completely model-independent manner for sources that lie on the FP, using Equation (4) once the values of C and D have been obtained from best-fit FP values a, b, and c for that sample of sources. The beam powers for the FP samples considered here are obtained using the values of C and D listed in Columns (2) and (9) of Table 1 of D18. No specific detailed model relating the compact radio luminosity to beam power is required to obtain these beam powers. The normalization from the FR II beam powers does enter through the parameter B determined with FR II AGNs (see D16 and D18). Because the normalization of the beam powers for FP sources is tied to that for the FR II sources, any shift caused by an offset of this normalization from the true value affects all of the sources in the same manner. This will be important later when the overall normalization of the beam powers, g_j, is discussed. Any normalization offset of the empirically determined beam powers from the true value will be absorbed by the normalization factor g_j, since it is the quantity (L_j/g_j) that enters into the determination of the black hole spin function.

Several authors have investigated whether the X-ray emission associated with FP sources is disk or jet emission (e.g., see the summary by Yuan & Narayan 2014). Both empirical and theoretical studies indicate that the X-ray emission arises from the accretion disk emission except in cases of very low X-ray luminosities, luminosities in Eddington units of less than about 10^{-6} (M03; Yuan & Cui 2005; Yuan & Narayan 2014; Xie & Yuan 2017); for the sources studied here, this could affect the results for only a few sources, notably for Sgr A*. In addition, S15 studied FP sources using [O III] luminosity rather than X-ray luminosity and found the same best-fit FP parameters, indicating that the X-ray emission originates from the accretion disk. Finally, the slope of the FL is very similar for FP sources (D18) and FR II AGNs (D16), and the bolometric luminosities of the FR II AGNs are based on [O III] luminosities. The value of the bolometric luminosity of the disk is obtained using Equation (5) with $\kappa_{\rm X} = 15.1$ (Ho 2009; D18). Given that all of the sources on the FP have black hole mass determinations, it is easy to construct the FL (given by Equation (1)) for separate samples, as was done by D18 for the NB16, S15, and M03 FP sources plus the FL sources studied by D16.

Here, the methods introduced by D16 are applied and extended to the four data sets for which the FL of black hole activity was studied (D16; D18). The application of these methods allows estimates of the spin function and spin of each black hole and the accretion disk magnetic field strength in

dimensionless and physical units of each source. Since these rely on the beam power, bolometric accretion disk luminosity, and black hole mass (or Eddington luminosity), these quantities are also included in the tables that list values of all quantities and are discussed in Section 2. Given the large numbers of sources included in the study, black hole demographics can be studied.

The data used for these studies are discussed in Section 2. The methods of obtaining the spin function, black hole spin, and accretion disk magnetic field strength are discussed in Section 3. The results are presented in Section 4, discussed in Section 5, and summarized in Section 6.

2. The Data

All quantities are obtained in a spatially flat cosmological model with two components, a mean mass density relative to the critical value at the current epoch of $\Omega_m = 0.3$ and a cosmological constant normalized by the critical density today of Ω_Λ =0.7; a value for Hubble's constant of $H_0 = 70\,\mathrm{km\,s^{-1}\,Mpc^{-1}}$ is assumed throughout.

The data sets studied here include the 576 LINERs from NB16, the 102 data points for four GBHs listed by S15, the 97 FR II sources from D16, and the 80 AGNs from M03. All four samples were studied in detail by D18. With the exception of a few black hole mass updates, the radio powers, X-ray luminosities, and black hole masses in the published source tables of NB16, S15, and M03 are used to obtain beam powers, bolometric luminosities, and Eddington luminosities as described in Section 1.1. For the sample of D16, these quantities are obtained as described in Section 1.1. Black hole masses have been updated for Sgr A^* (Ghez et al. 2008), Ark 564 (Vasudevan et al. 2016; Ilic et al. 2017), Mrk 335 (Grier et al. 2017), NGC 4051 (Seifina et al. 2018), NGC 4151 (Bentz et al. 2006), 3C 120 (Grier et al. 2017), NGC 1365 (Fazeli et al. 2019), GX 339−4 (King et al. 2013), XTE J118 +480 (Khargharia et al. 2013), and AO 6200 (Cantrell et al. 2010).

Note that the beam powers are obtained using the strong shock method for the D16 sources, while they are obtained using the "CD" method (given by Equation (4)) for the three other samples. The bolometric disk luminosities are obtained from the [O III] luminosity for the D16 sources, while they are obtained from X-ray luminosities for the other three samples. The sources studied by D16 are powerful extended classical double sources, while the radio sources in the other three samples are selected to have a powerful compact radio component. Yet all of the sources lie on the FL and have very similar best-fit FL parameters (D18). Interestingly, S15 showed that equivalent FP results are obtained when [O III] luminosity rather than X-ray luminosity is used as an indicator of the bolometric luminosity of AGNs.

A significant number of sources studied by D18 have beam powers one to two orders of magnitude larger than the bolometric luminosity of the disk. For these sources, it is reasonable to suppose that the outflow is powered, at least in part, by the spin of the black hole. Since the slope of the relationship indicated by Equation (1) is nearly identical for all samples studied, it is reasonable to conclude that all of the sources are governed by the same physics, and hence that the outflow of each of the sources is powered, at least in part, by the spin of the hole.

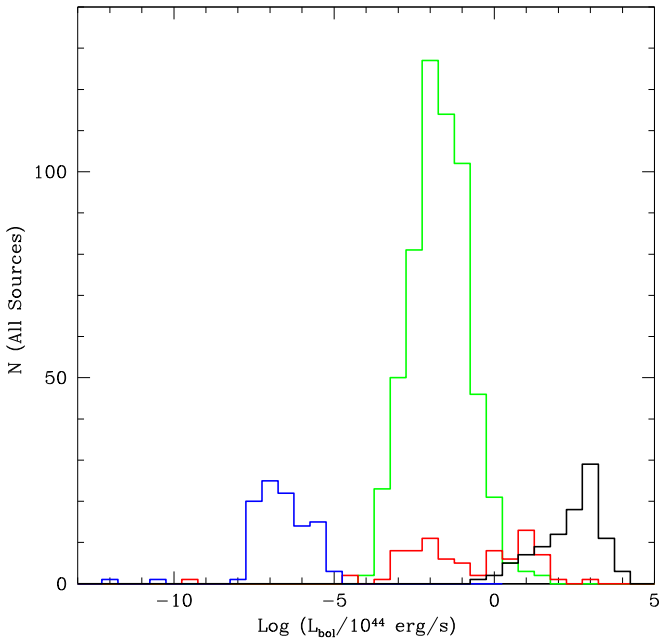

Figure 1. Histograms of the bolometric luminosity for each of the four samples studied here. Here and throughout the paper, the 576 LINERs from NB16 are shown in green, the 97 FR II sources from D16 are shown in black, the 80 AGNs from M03 are shown in red, and the 102 GBHs from S15 are shown in blue. The mean value and standard deviations of the distributions are −1.69 ± 0.90 (576 LINERs from NB16), 2.36 ± 0.97 (97 FR II sources from D16), −0.89 ± 1.99 (80 compact radio sources from M03), and −6.64 ± 0.97 (102 GBHs from S15).

The key quantities used to solve for parameter values characterizing the disk magnetic field strength and black hole spin of each source are the bolometric disk luminosity, $L_{\rm bol}$, beam power, L_j, and black hole mass, parameterized by the Eddington luminosity, $L_{\rm Edd}$. All quantities are obtained as described in Section 1.1. Histograms of $L_{\rm bol}$, L_j, $L_{\rm Edd}$, $L_{\rm bol}/L_{\rm Edd}$, $L_j/L_{\rm Edd}$, $L_{\rm Tot}/L_{\rm Edd}$, and $L_j/L_{\rm bol}$ are shown in Figures 1–7; $L_{\rm Tot} = L_{\rm bol} + L_j$ represents the total power produced by the source.

The uncertainties of $L_{\rm bol}$, L_j, and $L_{\rm Edd}$ factor into the uncertainties of the quantities discussed in Sections 1.1 and 3–5. The uncertainty of the log of the bolometric accretion disk luminosity, $\delta{\rm Log}(L_{\rm bol})$, obtained from the [O III] luminosity, applicable to the FR II sources, is about 0.38 (Heckman et al. 2004). In addition, $\delta{\rm Log}(L_{\rm bol})$ for FP sources obtained from the (2–10) keV luminosity is about 0.27 (D18), which is obtained by multiplying the uncertainty of the mean of 0.03 by the square root of the number of sources (80) included in the study to obtain the uncertainty per source. The uncertainties of the beam powers for the representative sample of FR II sources listed in O'Dea et al. (2009) are approximately $(\delta L_j)/L_j \simeq 0.3$, which translates to an uncertainty of the log of the beam power, $\delta{\rm Log}(L_j) \simeq 0.13$. Values of $\delta{\rm Log}(L_j)$ for the FP sources obtained as described by D18 are estimated to be about 0.16 for the LINERs, 0.24 for the M03 sources, and 0.07 for the GBHs; these were estimated by scaling the uncertainty of 0.13 for FR II AGNs by the ratio of the FL dispersions listed in Column (5) of Table 2 of D18 relative to the value for FR II AGNs. Black hole masses are obtained using different methods for each of the four samples studied. For the NB16 LINERs, the black hole masses are obtained using the Sloan Digital Sky Survey galaxy velocity dispersion σ and applying the McConnell & Ma (2013) relation to obtain the black hole

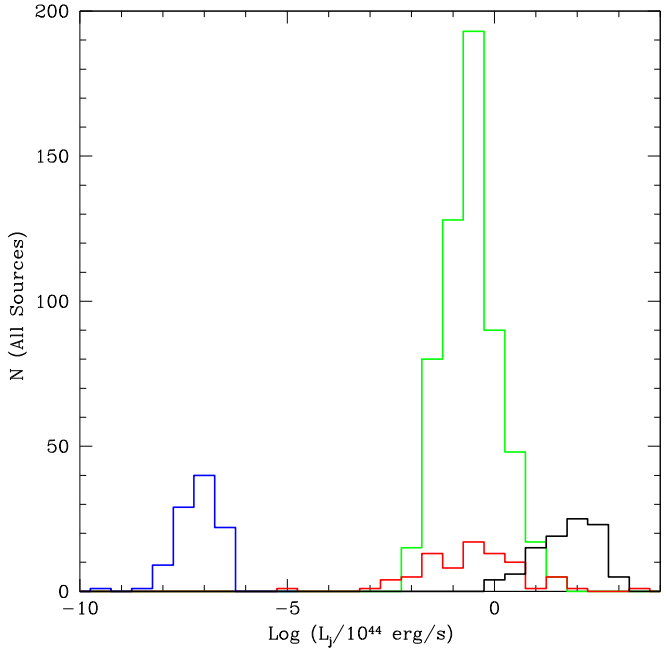

Figure 2. Histograms of the beam power for each of the four samples studied here; the sample colors are as in Figure 1. The mean value and standard deviations of the distributions are -0.55 ± 0.67 (576 LINERs from NB16), 1.71 ± 0.75 (97 FR II sources from D16), -0.54 ± 1.25 (80 compact radio sources from M03), and -7.15 ± 0.49 (102 GBHs from S15).

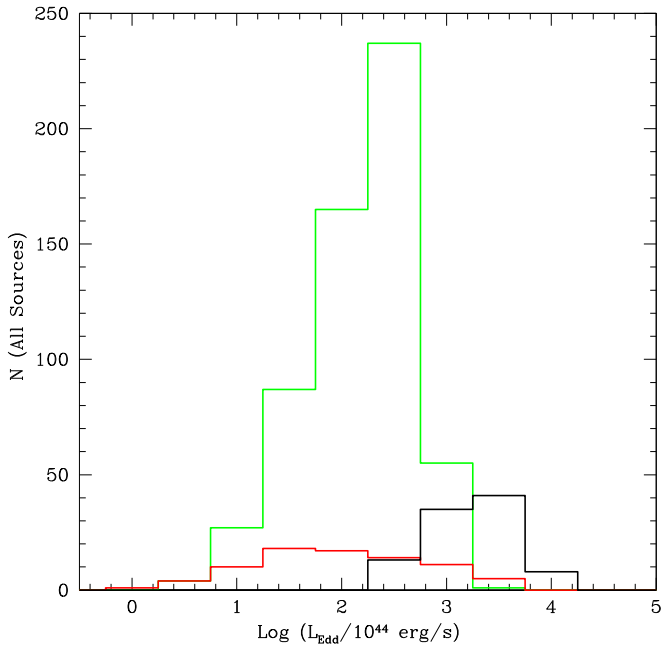

Figure 3. Histograms of the Eddington luminosity are shown for each of the three AGN samples studied here; the sample colors are as in Figure 1. The mean value and standard deviations of the distributions are 2.19 ± 0.50 (576 LINERs from NB16), 3.24 ± 0.40 (97 FR II sources from D16), 1.95 ± 0.81 (80 compact radio sources from M03), and -5.07 ± 0.09 (102 GBHs from S15), though these are not shown in the figure.

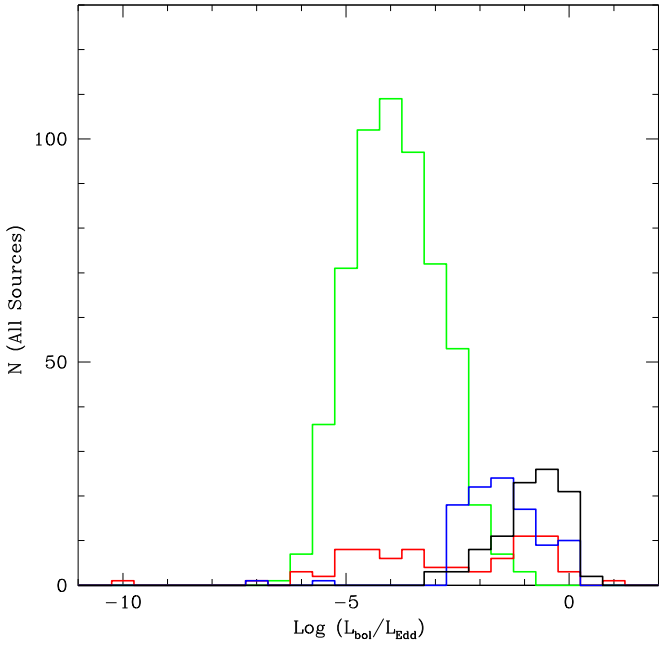

Figure 4. Histograms of the Eddington-normalized bolometric luminosity for each of the four samples studied here; the sample colors are as in Figure 1. The mean value and standard deviations of the distributions are -3.88 ± 0.98 (576 LINERs from NB16), -0.88 ± 0.77 (97 FR II sources from D16), -2.84 ± 2.06 (80 compact radio sources from M03), and -1.57 ± 0.98 (102 GBHs from S15).

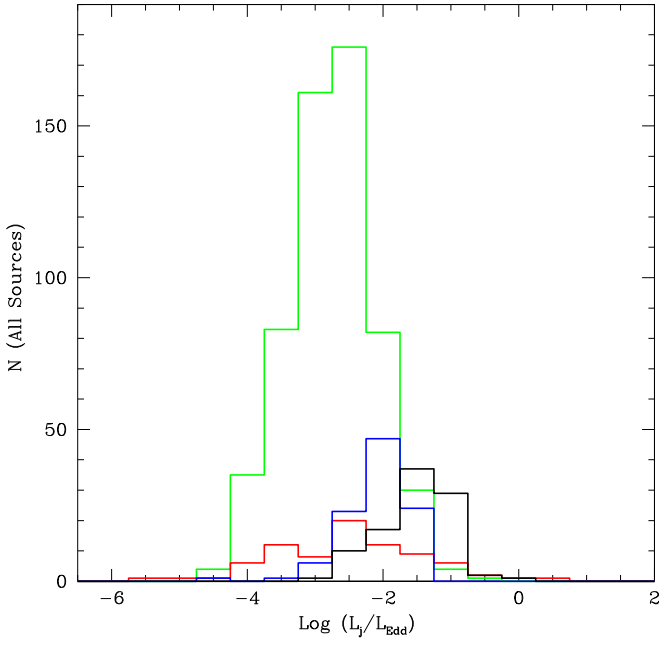

Figure 5. Histograms of the Eddington-normalized beam power are shown for each of the four samples studied here; the sample colors are as in Figure 1. The mean value and standard deviations of the distributions are -2.74 ± 0.63 (576 LINERs from NB16), -1.53 ± 0.51 (97 FR II sources from D16), -2.50 ± 1.11 (80 compact radio sources from M03), and -2.07 ± 0.50 (102 GBHs from S15).

mass of each source; the uncertainty is estimated to be about $\delta\mathrm{Log}(L_{\mathrm{Edd}}) \simeq 0.3$–$0.4$ for typical masses of these black holes, with the uncertainty increasing with black hole mass. For the M03 sample, the black hole masses are obtained using the relationship between black hole mass and galaxy velocity dispersion from Ferrarese & Merritt (2000) and updated by Ferrarese (2002), which has an uncertainty of about $\delta\mathrm{Log}(L_{\mathrm{Edd}}) \simeq 0.5$. For the FR II radio sources, $\delta\mathrm{Log}(L_{\mathrm{Edd}})$ is about 0.3 for the radio galaxies obtained from McLure et al. (2004), about 0.3 for a source at a redshift of about 1 for the radio galaxies obtained from McLure et al. (2006), and 0.4 for the radio-loud quasars obtained from McLure et al. (2006).

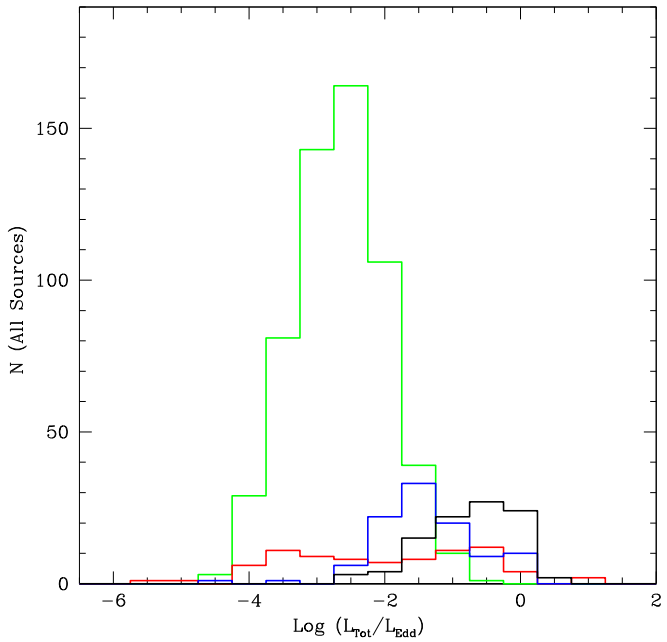

Figure 6. Histograms of the Eddington-normalized total source power, where the total source power or luminosity is the sum of the bolometric luminosity and the beam power, for each of the four samples studied here; the sample colors are as in Figure 1. The mean value and standard deviations of the distributions are -2.66 ± 0.67 (576 LINERs from NB16), -0.73 ± 0.66 (97 FR II sources from D16), -2.01 ± 1.40 (80 compact radio sources from M03), and -1.39 ± 0.75 (102 GBHs from S15).

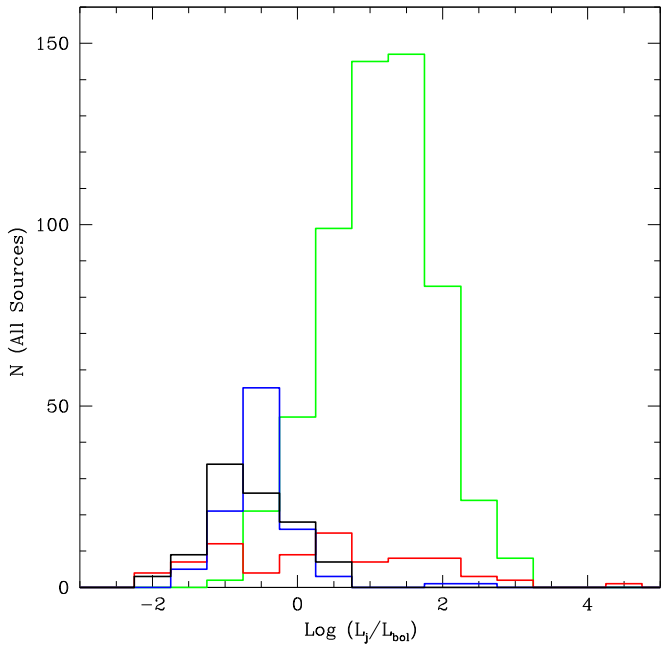

Figure 7. Histograms of the ratio of the beam power to the bolometric luminosity of the accretion disk for each of the four samples studied here; the sample colors are as in Figure 1. The mean value and standard deviations of the distributions are 1.14 ± 0.73 (576 LINERs from NB16), -0.65 ± 0.57 (97 FR II sources from D16), 0.35 ± 1.40 (80 compact radio sources from M03), and -0.50 ± 0.56 (102 GBHs from S15).

Note that for any quantity x, $\delta\mathrm{Log}(x) = (\delta x/x)(1/\mathrm{Ln}(10))$, so adding fractional uncerainties such as $(\delta x/x)$ in quadrature to obtain a total uncertainty translates into adding terms such as $\delta\mathrm{Log}(x)$ in quadrature to obtain the total uncertainty of the log of a quantity that depends on more than one factor. For the GBH a mass uncertainty of about $\delta\mathrm{Log}(L_{\mathrm{Edd}}) \simeq 0.037$ is indicated by Khargharia et al. (2013) for XTE J118+480, and $\delta\mathrm{Log}(L_{\mathrm{Edd}}) \simeq 0.016$ is indicated by Cantrell et al. (2010) for AO 6200; in addition, when considering data on one particular GBH, the variation of the mass term should be set to zero. These uncertainties of the mass are quite small relative to the uncertainties of the beam power and disk bolometric luminosity and thus can be ignored for the GBH.

3. The Method

The method introduced by D16 and expanded here is explained in Section 3.1. A more intuitive approach to the derivation of the key equations is presented in Section 3.2; the model assumptions are explained, and it is shown that results obtained regarding the properties of the accretion disk are independent of those obtained for black hole spins. The method and the inputs to the method are all empirically based, and thus the results can be applied to study and constrain specific accretion disk and jet models, as explained in Section 3.3. The uncertainties of the accretion disk properties and the black hole spin properties are also discussed in Section 3.3.

3.1. The Method—Part 1

All of the sources considered here fall on the FL of black hole activity, and the source properties indicate that the outflow is likely to be powered at least in part by the spin of the black hole, as discussed in Section 2. Thus, the beam power may be written as $L_j \propto \dot{m}\, M\, f(j) \propto B_p^2\, M^2\, f(j)$ (e.g., Blandford & Znajek 1977; Blandford 1990; Meier 1999; Yuan & Narayan 2014). Writing the bolometric luminosity of the disk as $L_{\mathrm{bol}} \propto \epsilon\, \dot{m}\, M$, and applying the empirical relationship given by Equation (1), leads to a derivation very similar to that presented in Section 1.1, and it is easy to show that Equation (2) results. A second, more intuitive derivation of Equations (2) and (7) is discussed in Part 2 of this section.

As described in Section 1.1, the maximum power of the accretion disk, $L_{\mathrm{bol}}(\mathrm{max})$, and that of the outflow, $L_j(\mathrm{max})$, are parameterized by the quantities g_{bol} and g_j, respectively: $L_{\mathrm{bol}}(\mathrm{max}) = g_{\mathrm{bol}} L_{\mathrm{Edd}}$ and $L_j(\mathrm{max}) = g_j L_{\mathrm{Edd}}$. The values of the normalization factors can be estimated empirically (see D16 and D18) and can also be guided by theoretical considerations. The Eddington magnetic field strength, B_{Edd}, of a black hole system is $B_{\mathrm{Edd}}^2 \propto M^{-1}$ (e.g., Rees 1984; Blandford 1990; Dermer et al. 2008), and, of course, $L_{\mathrm{Edd}} \propto M$. (The Eddington magnetic field B_{Edd} will have a pressure similar to that of a radiation field with the Eddington luminosity.) Thus, the beam power has the form

$$\left(\frac{L_j}{L_{\mathrm{Edd}}}\right) = g_j \left(\frac{B}{B_{\mathrm{Edd}}}\right)^2 \left(\frac{f(j)}{f_{\mathrm{max}}}\right), \tag{6}$$

where B is the total accretion disk magnetic field strength. If the energy density of the poloidal component of the magnetic field, B_p, is about one-third of the total energy density of the field, then the maximum possible value of g_j is one-third. Many factors related to empirical and theoretical considerations can affect the value of g_j, as discussed in Section 4.

Combining Equations (2) and (6), we obtain

$$\left(\frac{B}{B_{\mathrm{Edd}}}\right)^2 = \left(\frac{L_{\mathrm{bol}}}{g_{\mathrm{bol}} L_{\mathrm{Edd}}}\right)^A. \tag{7}$$

Thus, for sources that fall on the FL, the slope of the FL, A, for that sample can be substituted into Equation (7) to obtain an empirical determination of the magnetic field strength B in Eddington units. Note that a comparison of the equations described above indicates that $(B/B_{\rm Edd})^2$ is identified with the dimensionless mass accretion rate, $\dot{m}$, $\dot{m} \propto (B/B_{\rm Edd})^2$, with a constant of proportionality of order unity. The value of A may be obtained by a direct fit to Equation (1), as was done by D16 and D18, or by using the relationship between A and best-fit FP parameters included in Equation (3): $A = a/(a+b)$ (D18).

In addition, the total magnetic field strength B can then be obtained from the equation

$$\left(\frac{B}{10^4\ {\rm G}}\right) = \left(\frac{B}{B_{\rm Edd}}\right)\left(\frac{\kappa_B^2}{M_8}\right)^{1/2} = \left(\frac{L_{\rm bol}}{g_{\rm bol} L_{\rm Edd}}\right)^{A/2}\left(\frac{\kappa_B^2}{M_8}\right)^{1/2}, \quad (8)$$

where the Eddington magnetic field strength in units of 10^4 G is $B_{\rm Edd,4} \equiv \kappa_B M_8^{-1/2}$, where $\kappa_B \simeq 6$ (e.g., Rees 1984; Blandford 1990; Dermer et al. 2008).

3.2. The Method—Part 2

There is a second way to derive Equations (2) and (7), the key equations used to empirically quantify the properties of the accretion disk and black hole spin. This will illustrate the independence of the Eddington-normalized field strength $(B/B_{\rm Edd})$ and normalized spin function $(f(j)/f_{\rm max})$ obtained with the method applied here. The key assumption is that the outflow is powered at least in part by the spin of the black hole, as in the Blandford & Znajek mechanism (1977) and the closely related Meier mechanism (1999), both of which have the functional form given by Equation (6).

Equation (6) shows that the normalized beam power $[L_j/(g_j\ L_{\rm Edd})]$ is separable into two independent parts: $(B/B_{\rm Edd})^2$ and $(f(j)/f_{\rm max})$. The first part, $(B/B_{\rm Edd})^2$, depends on the properties of the accretion disk, since the magnetic field B that threads the ergosphere of the black hole is anchored in the accretion disk. The second part, $(f(j)/f_{\rm max})$, depends only on the spin of the black hole and is normalized by the maximum value of the spin function.

Thus, the assumptions are that the collimated outflow is powered at least in part by the spin of the black hole, which leads to Equation (6); that the strength of the poloidal component of the magnetic field that is threading the black hole and is anchored in the accretion disk is independent of the black hole spin; and that the spin of the black hole is independent of the conditions in the accretion disk. Thus, it is assumed that $(B/B_{\rm Edd})$ and $(f(j)/f_{\rm max})$ are independent. (Note that the poloidal component of the magnetic field is some fraction of the full field strength B, as discussed in Sections 3.1 and 4.)

Next, we note that four samples, including a sample of powerful extended radio sources and three samples of compact radio sources that fall on the FP, have an empirically determined relationship of the form $[L_j/L_{\rm Edd}] \propto [L_{\rm bol}/(g_{\rm bol} L_{\rm Edd})]^A$, which follows from Equation (1) with the disk normalization factor included. This empirical relationship only involves the properties of the accretion disk, indicated by the right-hand side of the equation, and the properties of the outflow, indicated by the left-hand side of the equation; the spin is not included in this empirically determined relationship. The term $[L_{\rm bol}/(g_{\rm bol} L_{\rm Edd})]^A$ is identified with the term $(B/B_{\rm Edd})^2$ on the right-hand side of Equation (6), that is, $(B/B_{\rm Edd})^2 = [L_{\rm bol}/(g_{\rm bol}\ L_{\rm Edd})]^A$, which is Equation (7). This is valid because it is assumed that the spin of the black hole is independent of the accretion disk properties. Substituting Equation (7) into Equation (6) leads to Equation (2).

This alternative derivation makes it clear that the field strength obtained with Equation (7) or Equation (8) is independent of the spin obtained with Equation (2) given the assumption that the outflow is described by Equation (6), and thus is separable into two independent functions, $(B/B_{\rm Edd})^2$ and $(f(j)/f_{\rm max})$. When these functions are obtained empirically, it is easy to check and confirm that there is no covariance between them, which indeed turns out to be the case.

3.3. The Method—Part 3

The "outflow method" of estimating black hole spins and accretion disk magnetic field strengths proposed by D16 and extended here can only be applied to certain categories of sources, as described in Section 1.1. It is an empirically based method and thus is independent of a specific accretion disk emission model and is independent of a specific jet model relating beam power to compact radio luminosity. The key assumptions are described in Section 3.2.

The sources selected for study follow the FL of black hole activity, given by Equation (1) (see D18 for other forms of this equation). This includes sources that were placed directly on the FL, such as the FR II sources, and FP sources, as described in Section 1.1. This means that the sources are empirically well described by only a few parameters. As it turns out, the samples studied are described by similar parameter values over a very large range of parameter space (described here by the parameter A) and thus are likely to be controlled by similar physical processes, as has been recognized for FP sources for quite some time (e.g., Corbel et al. 2003; Gallo et al. 2003; M03; Falcke et al. 2004; Körding et al. 2006a, 2006b; Gültekin et al. 2009; Bonchi et al. 2013; van Velzen & Falcke 2013; S15; NB16).

Thus, these sources are likely to have a special set of characteristics. For example, it is likely that the accretion disk magnetic field strength B either is in equipartition with the gas and radiation pressure P of the accretion disk or is some constant fraction of this pressure, so $P \propto B^2$ (e.g., Balbus & Hawley 1991, 1998; Hawley & Balbus 1991); that the magnetic field is threading the ergosphere of the black hole (a requirement for the spin-powered outflow model); and that the black holes have substantial spin. Substantial spin is required because the outflow beam power is proportional to the square of the black hole spin, so black holes with low spin will produce weak outflows via this process, as discussed in Section 6.

This means that the empirical results, once obtained, can be applied to study and constrain detailed outflow and accretion disk models since these models are not an input to any of the results presented here. That is, the gas and radiation pressure of the disk can be estimated from the quantity B^2 obtained using Equation (8), and the relationship between the bolometric disk luminosity, the disk pressure P, and the black hole mass can then be studied using Equation (7) or Equation (8). For example, Equation (7) indicates that $(B/B_{\rm Edd})^2 \simeq \dot{m} \simeq (L_{\rm bol}/L_{\rm Edd})^{1/2}$ for $g_{\rm bol} = 1$ and $A \simeq 0.5$ (see Tables 1 and 2 in D18), which is consistent with expectations of radiatively inefficient accretion disk models (see, e.g., Equation (4) of Ho 2009), though these

models may have to be extended or modified to allow values as high as $L_{\rm bol} \sim L_{\rm Edd}$ (e.g., Yuan & Narayan 2014). Similarly, the beam power for the FP sources is obtained by D18, as described in Section 1.1, without specifying a detailed physical model for the jet or for the relationship between the beam power and the radio luminosity of the compact radio source. The beam power is empirically determined using Equation (4). Thus, detailed physical jet models that reproduce the observed radio emission given the beam power could be explored, such as the models discussed by Heinz & Sunyaev (2003), M03, Heinz (2004), Yuan & Cui (2005), Yuan et al. (2005), and Li et al. (2008), for example.

The uncertainties of the input parameters $L_{\rm bol}$, L_j, and $L_{\rm Edd}$ will impact the uncertainties of $(B/B_{\rm Edd})$, $(B/10^4\,{\rm G})$, and $\sqrt{(f(j)/f_{\rm max})}$. To compute these uncertainties, we adopt a value of $A \simeq 0.45$ for all sources and use the shorthand $B_4 \equiv B/(10^4\,{\rm G})$ and $F \equiv \sqrt{(f(j)/f_{\rm max})}$. Following the discussion provided at the end of Section 2, and considering Equation (7), it is easy to show that $\delta{\rm Log}(B/B_{\rm Edd}) = (A/2)\,[(\delta{\rm Log}(L_{\rm bol}))^2 + (\delta{\rm Log}(L_{\rm Edd}))^2]^{1/2}$, so for FR II AGNs with $\delta{\rm Log}(L_{\rm Edd}) \simeq 0.3$ and 0.4, we obtain $\delta{\rm Log}(B/B_{\rm Edd}) \simeq 0.11$ and 0.12, respectively. It is assumed that $g_{\rm bol} = 1$ for all sources, that is, the maximum possible luminosity of the disk is equal to the Eddington luminosity, which is consistent with the samples studied here, as discussed by D16 and D18. Adopting values of $\delta{\rm Log}(L_{\rm Edd}) \simeq 0.3-0.4$ for the LINERs, we obtain $\delta{\rm Log}(B/B_{\rm Edd}) \simeq 0.09$ and 0.11, respectively. For FP sources with $\delta{\rm Log}(L_{\rm Edd}) \simeq 0.5$, such as the M03 sources, $\delta{\rm Log}(B/B_{\rm Edd}) \simeq 0.13$. For the GBHs, $\delta{\rm Log}(B/B_{\rm Edd}) \simeq 0.06$. For the magnetic field strength in physical units, Equation (8) indicates $\delta{\rm Log}(B_4) = [(A/2)^2\,(\delta{\rm Log}(L_{\rm bol}))^2 + [(A+1)/2]^2(\delta{\rm Log}(L_{\rm Edd}))^2]^{1/2}$, so $\delta{\rm Log}(B_4) \simeq 0.23$, 0.22, and 0.37 for the FR II AGNs, LINERs, and M03 sources, respectively, adopting $\delta{\rm Log}(L_{\rm Edd}) \simeq 0.3$ for the LINERs and FR II AGNs and $\delta{\rm Log}(L_{\rm Edd}) \simeq 0.5$ for the M03 sources. For a value of $\delta{\rm Log}(L_{\rm Edd}) \simeq 0.4$ for the FR II AGNs and LINERs, these values become 0.30 for both FR II AGNs and LINERs. For the GBHs, $\delta{\rm Log}(B_4) \simeq 0.06$. Equation (2) indicates that $\delta{\rm Log}(F) = 0.5\,[(\delta{\rm Log}(L_j))^2 + (\delta{\rm Log}(g_j))^2 + (A-1)^2\,(\delta{\rm Log}(L_{\rm Edd}))^2 + A^2(\delta{\rm Log}(L_{\rm bol}))^2]^{1/2}$. Leaving aside $(\delta g_j/g_j)$ for the present time, for the FR II AGNs, $\delta{\rm Log}(F) \simeq 0.14$ and 0.15 for $\delta{\rm Log}(L_{\rm Edd}) \simeq 0.3$ and 0.4, respectively. For the LINERs, $\delta{\rm Log}(F) \simeq 0.13$ and 0.15 for $\delta{\rm Log}(L_{\rm Edd}) \simeq 0.3$ and 0.4, respectively. For the M03 sources, $\delta{\rm Log}(F) \simeq 0.19$. For the GBHs, $\delta{\rm Log}(F) \simeq 0.07$. These estimated uncertainties per source are included in parentheses in Columns (4), (7), and (8) in the top part of Table 1.

4. Results

The spin function, $f(j)/f_{\rm max}$, is obtained using Equation (2); the accretion disk magnetic field strength in Eddington units, $(B/B_{\rm Edd})$, is obtained using Equation (7); and the magnetic field strength is obtained in physical units using Equation (8) for each source. Once obtained, it turns out that there is no covariance between the spin function and either of the field strengths; they are independent, as expected (see Section 3.2). Results for each sample and some specific sources are summarized in Table 1.

Source parameters are obtained as described in Sections 1–3. These parameters, including name, type, redshift or distance, Eddington luminosity, beam power, bolometric luminosity, square root of the normalized spin function, black hole spin, Eddington-normalized magnetic field strength, and magnetic field strength in units of 10^4 G, are listed in Tables 2–5 for each of the samples studied; all luminosities are in erg s^{-1}. Results are also displayed in Figures 8–14, and the mean values and dispersions of the histograms are summarized in Table 1. This table also includes information on each of the four GBH systems, Sgr A*, M87, and six AGN systems that have spin values obtained with the X-ray reflection method; systems described by Reynolds (2019) as having "robust" spin values that overlap with the sources studied here are included in Table 1. Three W galaxies from Grimes et al. (2004) are also included at the end of Table 4, and a second observation of AO 6200 is discussed in Section 5.

The values of $g_{\rm bol}$ and g_j can be inferred empirically. The empirical results presented by D16 and D18 suggest that $g_{\rm bol} \simeq 1$ and $g_j \simeq 0.1$; these values are adopted here. It is easy to scale the results for other values of these parameters. As discussed in Section 3.1, theoretical considerations suggest a maximum value of g_j of about one-third, and other factors can also affect the value of g_j. Empirically, there could be a normalization offset of the value of L_j from the true value, and this would be absorbed into the value of g_j when this is determined by the maximum measured value of $L_j/L_{\rm Edd}$. In addition, there may be variations in the ratio of $(B_p/B)^2$, leading to variations in the parameter g_j. Interestingly, the values of g_j indicated by the Meier (1999) model are $g_j \simeq 0.3$ for $(B_p/B)^2 \simeq 1$ and $g_j \simeq 0.1$ for $(B_p/B)^2 \simeq 1/3$. This can be seen by considering Equation (1) of Daly (2011), noting that the magnetic field in that equation is the poloidal component only, replacing j with $\sqrt{f(j)/f_{\rm max}}$, and writing the equation in the form of Equation (6). Thus, variations in the fraction of the total magnetic field that is in the poloidal component cause variations in g_j, which would affect determinations of $\sqrt{f(j)/f_{\rm max}}$ and hence j. As g_j increases from the value of 0.1 adopted here, the values of $\sqrt{f(j)/f_{\rm max}}$ and hence j will decrease from the values listed here. For $1/3 \leqslant (B_p/B)^2 \leqslant 1$, this limits the range of values of g_j to 0.1–0.3 in the context of the Meier (1999) model.

The spin function $f(j)/f_{\rm max}$ is obtained using Equation (2), and the Eddington-normalized magnetic field strength $(B/B_{\rm Edd})$ is obtained using Equation (7) applying the value of A listed in Column (3) of Table 2 of D18 for each of the four samples considered here. Values of the spin function and Eddington-normalized magnetic field are illustrated in Figure 8. The cutoff of the sources at $(B/B_{\rm Edd})^2 \simeq 1$ reflects the cutoff of sources at $L_{\rm bol} \simeq L_{\rm Edd}$, as discussed by D16 and D18. Statistical fluctuations and measurement uncertainties allow sources to have values of $f(j)/f_{\rm max} > 1$.

The GBH systems have multiple simultaneous radio and X-ray measurements; the values used here are from S15, who obtained them from Corbel et al. (2013) for GX 339−4, Corbel et al. (2008) for V404 Cyg, Wagner et al. (2001) for XTE J1118+480, and Gallo et al. (2006) for AO 6200. Each set of measurements yields a value of the spin function and magnetic field strength, as shown in Figures 8, 9, and 12 and summarized in Table 1. As can be seen in Figure 9, the measurements for each source tend to cluster around a specific value of the spin function, and, in general, the spin functions tend to have a smaller dispersion than the magnetic field strengths; these differences are evident in the mean values and dispersions listed in Table 1. It is interesting that AO 6200 has a much lower magnetic field strength but a similar spin value compared with the other GBH. (Another observation of this source from

Table 1
Mean Value and Standard Deviation of Histograms and Values for Select Individual Sources[a]

Sample (1)	Type (2)	N[b] (3)	$\mathrm{Log}\sqrt{(f(j)/f_{\max})}$ (4)	j (5)	j_{pub} (ref)[c] (6)	$\mathrm{Log}(B/B_{\mathrm{Edd}})$ (7)	$\mathrm{Log}(B/10^4\ \mathrm{G})$ (8)
NB16(1)[d]	AGN	576	-0.04 ± 0.24 (0.14)	0.93 ± 0.10		-0.83 ± 0.21 (0.10)	-0.09 ± 0.39 (0.22)
D16	AGN	97	-0.07 ± 0.19 (0.15)	0.93 ± 0.11		-0.19 ± 0.17 (0.12)	0.03 ± 0.23 (0.23)
M03	AGN	80	-0.17 ± 0.36 (0.19)	0.81 ± 0.20		-0.58 ± 0.42 (0.13)	0.27 ± 0.66 (0.37)
S15	GBH	102	-0.17 ± 0.10 (0.07)	0.92 ± 0.09		-0.37 ± 0.23 (0.06)	4.00 ± 0.24 (0.06)
GX 339−4	GBH	76	-0.17 ± 0.06	0.92 ± 0.06	0.94 ± 0.02 (1)	-0.32 ± 0.18	4.07 ± 0.18
GX 339−4					$0.95^{+0.03}_{-0.05}$ (2)		
V404 Cyg	GBH	20	-0.10 ± 0.06	0.97 ± 0.02		-0.44 ± 0.24	3.84 ± 0.24
XTE J1118[e]	GBH	5	-0.43 ± 0.01	0.66 ± 0.02		-0.54 ± 0.01	3.80 ± 0.01
AO 6200[f]	GBH	1	-0.08 ± 0.07	0.98 ± 0.07		-1.62 ± 0.06	2.76 ± 0.06
Sgr A^*	AGN	1	-0.17 ± 0.19	0.93 ± 0.15		-2.09 ± 0.13	-0.61 ± 0.37
M87[g]	AGN	1	0.13 ± 0.19	1.00 ± 0.15		-1.19 ± 0.13	-1.16 ± 0.37
Ark 564	AGN	1	0.06 ± 0.19	1.00 ± 0.15	$0.96^{+0.01}_{-0.11}$ (3)	0.17 ± 0.13	1.93 ± 0.37
Mrk 335	AGN	1	-0.29 ± 0.19	0.81 ± 0.15	>0.91 (3)	-0.15 ± 0.13	1.06 ± 0.37
Mrk 335					$0.70^{+0.12}_{-0.01}$ (4)		
Mrk 335					$0.83^{+0.10}_{-0.13}$ (5)		
NGC 1365	AGN	1	0.53 ± 0.19	1.00 ± 0.15	>0.84 (3)	-0.64 ± 0.13	0.70 ± 0.37
NGC 4051	AGN	1	-0.02 ± 0.19	1.00 ± 0.15	>0.99 (3)	-0.34 ± 0.13	1.30 ± 0.37
NGC 4151	AGN	1	-0.27 ± 0.19	0.84 ± 0.15	>0.9 (3)	-0.35 ± 0.13	0.60 ± 0.37
3C 120	AGN	1	0.59 ± 0.19	1.00 ± 0.15	>0.95 (3)	-0.13 ± 0.13	0.78 ± 0.37

Notes.
[a] Obtained for $g_{\mathrm{bol}} = 1$ and $g_j = 0.1$ for all sources. The estimated uncertainty per source is included in parentheses following the standard deviation in Columns (4), (7), and (8) for the samples listed in the top part of the table, as discussed in Section 3.3. The bottom part of the table includes entries for three individual GBHs, which have multiple observations per source, one additional GBH, and several individual AGNs.
[b] N is the number of sources for the AGNs and the number of measurements for the GBHs.
[c] Published spin values; the citations are (1) Miller et al. (2009), (2) García et al. (2015), (3) Vasudevan et al. (2016), (4) Patrick et al. (2012), and (5) Walton et al. (2013).
[d] Parameters are from the first line of Table 3 of NB16.
[e] The full source name is XTE J1118+480.
[f] The uncertainties for this source and the other individual sources listed here are estimated as described in Section 3.3.
[g] Also referred to as NGC 4486.

1975 to 1976 is discussed in Section 5 and indicates a similar spin value but a significantly higher field strength.) Having multiple observations per source allows a comparison of spin and magnetic field strength values for a particular GBH indicated by measurements obtained at different times. The spin indicators $\sqrt{(f(j)/f_{\max})}$ of GX 339−4 and V404 Cyg have a very small dispersion, while the dispersions of the magnetic field strengths are larger; recall that $\sqrt{(f(j)/f_{\max})} \propto j$ to first order in j, so this is the quantity studied here as described in Section 1.1. As will be discussed in Section 5, this suggests that the spin of the GBH remains constant (as expected), but the accretion disk magnetic field strength is time variable and varies as the accretion rate changes. This impacts the beam power of the outflow, since this is regulated in part by the magnetic field strength of the accretion disk.

The histograms of the black hole spin function are shown for each sample separately in Figure 10, and the mean values and dispersions of the histograms are listed in Table 1. All of the source types, including LINERs (NB16), powerful extended (FR II) radio sources (D16), compact radio sources that are AGNs (M03), and GBHs (S15), have similar spin function mean values. This indicates that source type is not related to black hole spin for the sources with collimated outflows studied here. This also indicates that black hole spin does not determine AGN type for the types of sources considered here.

This is consistent with the result obtained by D16 for FR II sources. D16 found that subtypes of FR II sources, including high-excitation radio galaxies (HEGs), low-excitation radio galaxies (LEGs), and radio-loud quasars (RLQs), had similar spin functions and spin function distributions. The results obtained here indicate that the mean value and dispersion of all quantities for each of the subsamples, including 55 HEGs, 29 RLQs, and 13 LEGs, are very similar to those of the full sample of 97 sources with the exception of $\mathrm{Log}(B/B_{\mathrm{eq}})$, which has values of -0.20 ± 0.16 for 55 HEGs, -0.09 ± 0.10 for 29 RLQs, and -0.39 ± 0.16 for 13 LEGs. That is, different FR II types are not distinguishable by mean value or dispersion of spin function, spin value, or magnetic field strength in physical units, indicating that black hole spin does not determine AGN type for these three types of classical double (FR II) sources.

Histograms of the accretion disk magnetic field strength in units of the Eddington field strength are shown Figure 11 and are obtained as described above. The mean values and dispersions of the field strength are listed in Table 1 and mirror those of the bolometric disk luminosity in Eddington units (see Equation (7)). There are a broad range of values of the Eddington-normalized disk magnetic field strength, as expected since this tracks the Eddington-normalized bolometric luminosity of the disk. Insofar as the Eddington-normalized disk luminosity varies with AGN type (e.g., Ho 2009), so does the

Table 2
Beam Power, Spin Parameters, and Disk Magnetic Field Strength Estimates for 102 Measurements of Four GBHs

Source (1)	Log ($L_{\rm Edd}$) (2)	Log (L_j) (3)	Log ($L_{\rm bol}$) (4)	Log $\left(\sqrt{\frac{f(j)}{f_{\rm max}}}\right)$ (5)	j (6)	Log ($B/B_{\rm Edd}$) (7)	Log ($B/10^4$ G) (8)
GX 339−4	38.89	37.08	38.06	−0.21	0.89	−0.19	4.19
GX 339−4	38.89	37.08	38.07	−0.21	0.89	−0.19	4.19
GX 339−4	38.89	37.02	37.64	−0.14	0.95	−0.29	4.09
GX 339−4	38.89	37.02	37.51	−0.11	0.97	−0.33	4.06
GX 339−4	38.89	36.62	36.94	−0.18	0.92	−0.46	3.93
GX 339−4	38.89	36.73	37.44	−0.24	0.87	−0.34	4.05
GX 339−4	38.89	37.05	38.02	−0.22	0.89	−0.20	4.18
GX 339−4	38.89	37.06	38.04	−0.22	0.89	−0.20	4.19
GX 339−4	38.89	36.91	37.33	−0.12	0.96	−0.37	4.02
GX 339−4	38.89	36.89	37.28	−0.12	0.96	−0.38	4.01
GX 339−4	38.89	37.14	37.71	−0.10	0.98	−0.28	4.11
GX 339−4	38.89	36.62	36.92	−0.17	0.92	−0.46	3.93
GX 339−4	38.89	37.19	38.21	−0.19	0.91	−0.16	4.23
GX 339−4	38.89	37.13	37.98	−0.16	0.93	−0.21	4.17
GX 339−4	38.89	36.80	37.37	−0.19	0.92	−0.36	4.03
GX 339−4	38.89	36.50	36.28	−0.08	0.98	−0.61	3.78
GX 339−4	38.89	37.07	37.84	−0.16	0.93	−0.25	4.14
GX 339−4	38.89	36.61	37.13	−0.23	0.88	−0.41	3.98
GX 339−4	38.89	36.57	37.01	−0.22	0.89	−0.44	3.95
GX 339−4	38.89	36.42	36.72	−0.22	0.88	−0.51	3.88
GX 339−4	38.89	36.58	37.00	−0.21	0.89	−0.44	3.94
GX 339−4	38.89	36.15	36.80	−0.38	0.71	−0.49	3.90
GX 339−4	38.89	36.39	36.44	−0.17	0.93	−0.57	3.81
GX 339−4	38.89	36.39	36.27	−0.13	0.95	−0.62	3.77
GX 339−4	38.89	36.58	36.76	−0.16	0.94	−0.50	3.89
GX 339−4	38.89	36.58	36.73	−0.14	0.95	−0.51	3.88
GX 339−4	38.89	36.15	36.56	−0.32	0.78	−0.55	3.84
GX 339−4	38.89	36.50	36.21	−0.06	0.99	−0.63	3.76
GX 339−4	38.89	36.89	37.38	−0.14	0.95	−0.36	4.03
GX 339−4	38.89	36.86	37.25	−0.13	0.96	−0.39	4.00
GX 339−4	38.89	37.02	37.39	−0.08	0.98	−0.35	4.03
GX 339−4	38.89	36.66	37.05	−0.18	0.92	−0.43	3.95
GX 339−4	38.89	36.75	37.16	−0.17	0.93	−0.41	3.98
GX 339−4	38.89	36.72	37.13	−0.17	0.93	−0.41	3.98
GX 339−4	38.89	36.85	37.26	−0.14	0.95	−0.38	4.01
GX 339−4	38.89	37.54	38.82	−0.16	0.94	−0.02	4.37
GX 339−4	38.89	37.51	38.80	−0.17	0.93	−0.02	4.37
GX 339−4	38.89	36.22	36.41	−0.25	0.85	−0.58	3.80
GX 339−4	38.89	36.57	36.93	−0.20	0.90	−0.46	3.93
GX 339−4	38.89	37.26	38.28	−0.17	0.93	−0.14	4.24
GX 339−4	38.89	37.23	38.28	−0.19	0.91	−0.14	4.25
GX 339−4	38.89	37.30	38.37	−0.17	0.93	−0.12	4.26
GX 339−4	38.89	37.32	38.40	−0.17	0.93	−0.11	4.27
GX 339−4	38.89	37.39	38.51	−0.16	0.94	−0.09	4.30
GX 339−4	38.89	37.43	38.58	−0.16	0.94	−0.07	4.32
GX 339−4	38.89	37.51	38.64	−0.13	0.95	−0.06	4.33
GX 339−4	38.89	37.56	38.67	−0.12	0.97	−0.05	4.34
GX 339−4	38.89	37.55	38.70	−0.13	0.96	−0.05	4.34
GX 339−4	38.89	37.50	38.71	−0.15	0.94	−0.04	4.35
GX 339−4	38.89	37.05	37.71	−0.14	0.95	−0.28	4.11
GX 339−4	38.89	37.16	38.42	−0.25	0.85	−0.11	4.28
GX 339−4	38.89	37.38	38.80	−0.23	0.87	−0.02	4.37
GX 339−4	38.89	37.23	38.55	−0.25	0.86	−0.08	4.31
GX 339−4	38.89	36.38	36.33	−0.15	0.94	−0.60	3.79
GX 339−4	38.89	36.43	36.50	−0.17	0.93	−0.56	3.83
GX 339−4	38.89	36.46	36.92	−0.25	0.85	−0.46	3.92
GX 339−4	38.89	36.35	36.46	−0.20	0.90	−0.57	3.82
GX 339−4	38.89	36.37	36.46	−0.19	0.91	−0.57	3.82
GX 339−4	38.89	36.82	37.46	−0.20	0.90	−0.34	4.05
GX 339−4	38.89	36.93	37.63	−0.18	0.92	−0.30	4.09
GX 339−4	38.89	36.72	37.19	−0.19	0.91	−0.40	3.99

Table 2
(Continued)

Source (1)	Log $(L_{\rm Edd})$ (2)	Log (L_j) (3)	Log $(L_{\rm bol})$ (4)	Log $\left(\sqrt{\frac{f(j)}{f_{\rm max}}}\right)$ (5)	j (6)	Log $(B/B_{\rm Edd})$ (7)	Log $(B/10^4\ {\rm G})$ (8)
GX 339−4	38.89	36.72	37.32	−0.22	0.89	−0.37	4.02
GX 339−4	38.89	36.73	37.17	−0.18	0.92	−0.40	3.98
GX 339−4	38.89	36.71	37.16	−0.18	0.92	−0.41	3.98
GX 339−4	38.89	37.13	37.70	−0.10	0.97	−0.28	4.11
GX 339−4	38.89	35.91	36.66	−0.47	0.61	−0.52	3.86
GX 339−4	38.89	36.85	37.05	−0.09	0.98	−0.43	3.96
GX 339−4	38.89	36.93	37.21	−0.08	0.98	−0.39	3.99
GX 339−4	38.89	36.98	37.37	−0.10	0.98	−0.36	4.03
GX 339−4	38.89	37.00	37.48	−0.11	0.97	−0.33	4.06
GX 339−4	38.89	37.03	37.57	−0.12	0.96	−0.31	4.08
GX 339−4	38.89	37.54	38.75	−0.15	0.95	−0.03	4.36
GX 339−4	38.89	37.53	38.72	−0.14	0.95	−0.04	4.35
GX 339−4	38.89	37.54	38.71	−0.13	0.96	−0.04	4.35
GX 339−4	38.89	36.63	36.85	−0.15	0.94	−0.48	3.91
GX 339−4	38.89	36.73	36.94	−0.13	0.96	−0.46	3.93
XTE J1118+480	38.99	36.05	36.75	−0.44	0.64	−0.53	3.81
XTE J1118+480	38.99	36.05	36.64	−0.42	0.67	−0.55	3.79
XTE J1118+480	38.99	36.05	36.65	−0.42	0.66	−0.55	3.79
XTE J1118+480	38.99	36.05	36.63	−0.42	0.67	−0.55	3.78
XTE J1118+480	38.99	36.05	36.74	−0.44	0.64	−0.53	3.81
V404 Cyg	39.11	37.28	37.97	−0.15	0.94	−0.27	4.01
V404 Cyg	39.11	35.65	33.59	0.07	1.00	−1.30	2.98
V404 Cyg	39.11	37.29	37.96	−0.14	0.95	−0.27	4.01
V404 Cyg	39.11	37.07	37.62	−0.17	0.93	−0.35	3.93
V404 Cyg	39.11	37.41	37.88	−0.06	0.99	−0.29	3.99
V404 Cyg	39.11	36.92	37.19	−0.14	0.95	−0.45	3.83
V404 Cyg	39.11	37.45	37.87	−0.04	1.00	−0.29	3.99
V404 Cyg	39.11	36.76	36.47	−0.05	0.99	−0.62	3.66
V404 Cyg	39.11	36.98	37.25	−0.13	0.96	−0.44	3.84
V404 Cyg	39.11	36.94	37.19	−0.13	0.96	−0.45	3.83
V404 Cyg	39.11	37.12	37.72	−0.17	0.93	−0.33	3.95
V404 Cyg	39.11	37.14	37.45	−0.09	0.98	−0.39	3.89
V404 Cyg	39.11	36.92	37.10	−0.12	0.96	−0.47	3.81
V404 Cyg	39.11	36.93	37.23	−0.15	0.94	−0.44	3.84
V404 Cyg	39.11	37.28	37.93	−0.14	0.95	−0.28	4.00
V404 Cyg	39.11	37.52	38.18	−0.08	0.99	−0.22	4.06
V404 Cyg	39.11	36.67	36.35	−0.07	0.99	−0.65	3.63
V404 Cyg	39.11	36.83	36.60	−0.05	0.99	−0.59	3.69
V404 Cyg	39.11	37.03	37.37	−0.13	0.96	−0.41	3.87
V404 Cyg	39.11	37.42	37.94	−0.07	0.99	−0.28	4.00
AO 6200	38.93	34.52	32.03	−0.08	0.98	−1.62	2.75

Notes. All luminosities are in erg s^{-1}.

(This table is available in its entirety in machine-readable form.)

Eddington-normalized magnetic field strength. As noted in Section 3.1, $\dot{m} \simeq (B/B_{\rm Edd})^2$, and Figure 8 indicates that the dimensionless mass accretion rate spans about 2.5 orders of magnitude, ranging from about 3×10^{-3} to 1, with sharp cutoffs at both the low and high ends. The cutoff at low values of $(L_{\rm bol}/L_{\rm Edd})$ is likely due to a survey flux limit (e.g., NB16 for the LINERs), while that at the high end occurs at $L_{\rm bol} \simeq L_{\rm Edd}$.

The black hole spin may be obtained from the spin function once a particular outflow model is adopted, and it is shown in Figure 12 for the values of g_j and $g_{\rm bol}$ adopted as described above. As discussed in Section 1.1, numerical simulations suggest that the conversion from the spin function to spin can change depending on the details of the model for the black hole system (e.g., Tchekhovskoy et al. 2010; Yuan & Narayan 2014), so this may be a source of uncertainty. Here, the standard conversion from the spin function to black hole spin, $\sqrt{f(j)/f_{\rm max}} = j(1+\sqrt{1-j^2})^{-1}$, is adopted. For $f(j)/f_{\rm max} \leqslant 1$, this implies

$$j = \frac{2\sqrt{f(j)/f_{\rm max}}}{f(j)/f_{\rm max}+1}. \quad (9)$$

The black hole spin is obtained using Equation (9), and values of $f(j)/f_{\rm max} > 1$ are set equal to 1. This causes asymmetries in the distribution of spin values when many sources have values of $f(j)/f_{\rm max} > 1$. Values of j thus obtained are shown in

Table 3
Beam Power, Spin Parameters, and Disk Magnetic Field Strength Estimates for 80 Compact Radio Sources. All luminosities are in erg s^{-1}

Source	Type	D	Log	Log	Log	Log $\sqrt{\left(\frac{f(j)}{f_{\max}}\right)}$	j	Log	Log
		(Mpc)	($L_{\rm Edd}$)	(L_j)	($L_{\rm bol}$)			($B/B_{\rm Edd}$)	($B/10^4$ G)
(1)	(2)	(3)	(4)	(5)	(6)	(7)	(8)	(9)	(10)
Ark 564	NS1	106	44.14	43.61	44.98	0.06	1.00	0.17	1.93
Cyg *A*	S2/L2	240	47.51	45.67	45.46	0.00	1.00	−0.42	−0.35
IC 1459	L2	31	47.11	44.42	41.90	0.22	1.00	−1.07	−0.80
IC 4296	L1.9	201	47.21	44.40	42.44	0.07	1.00	−0.98	−0.76
IC 4329*A*	S1	70	44.80	43.86	44.96	0.00	1.00	0.03	1.46
Mrk 3	S2	56	46.92	44.53	43.94	−0.09	0.98	−0.61	−0.24
Mrk 279	S1.5	136	45.73	43.75	44.96	−0.34	0.76	−0.16	0.80
Mrk 335	NS1	115	45.25	43.38	44.54	−0.29	0.81	−0.15	1.06
Mrk 348	S2	64	45.28	44.41	44.09	0.31	1.00	−0.25	0.94
Mrk 478	NS1	339	45.41	43.72	45.11	−0.28	0.82	−0.06	1.06
Mrk 507	NS1	231	45.21	43.75	44.21	−0.03	1.00	−0.21	1.02
Mrk 509	NS1	154	45.97	43.40	45.24	−0.64	0.44	−0.15	0.69
Mrk 590	S1.2	117	45.34	43.69	44.82	−0.22	0.88	−0.11	1.05
Mrk 766	NS1	55	44.75	43.41	44.14	−0.05	1.00	−0.13	1.33
NGC 315	L1.9	71	47.21	44.93	42.92	0.24	1.00	−0.88	−0.66
NGC 1052	L1.9	21	46.40	44.53	42.81	0.30	1.00	−0.74	−0.11
NGC 1068	S1.9	15	45.31	43.99	42.24	0.47	1.00	−0.63	0.54
NGC 1275	S2	75	46.75	45.89	44.64	0.50	1.00	−0.43	0.02
NGC 1365	S1.8	23	44.98	43.76	41.84	0.53	1.00	−0.64	0.70
NGC 1386	S2	12	45.31	42.24	41.88	−0.33	0.76	−0.70	0.47
NGC 1667	S2	66	46.04	42.70	41.29	−0.20	0.91	−0.98	−0.17
NGC 2110	S2	33	46.52	43.90	43.84	−0.26	0.84	−0.55	0.02
NGC 2273	S2	30	45.38	43.06	42.64	−0.10	0.97	−0.56	0.58
NGC 2787	L1.9	8	45.70	42.61	39.64	0.20	1.00	−1.24	−0.27
NGC 2841	L2	13	46.53	41.73	39.50	−0.46	0.62	−1.44	−0.88
NGC 2992	S2	33	45.86	43.64	43.34	−0.09	0.98	−0.52	0.38
NGC 3031	S1.5	4	45.90	42.33	41.14	−0.31	0.79	−0.98	−0.10
NGC 3079	S2	22	45.76	43.46	41.44	0.24	1.00	−0.89	0.06
NGC 3147	S2	44	46.90	43.19	42.85	−0.53	0.55	−0.83	−0.45
NGC 3169	L2	18	46.02	42.59	42.59	−0.51	0.56	−0.70	0.11
NGC 3226	L1.9	17	46.34	42.60	41.98	−0.48	0.60	−0.90	−0.24
NGC 3227	S1.5	22	45.70	43.14	43.23	−0.28	0.83	−0.51	0.47
NGC 3516	S1	42	45.47	43.17	44.44	−0.44	0.64	−0.21	0.88
NGC 3998	L1.9	15	46.86	43.17	42.90	−0.54	0.54	−0.81	−0.42
NGC 4051	NS1	18	44.38	42.67	42.74	−0.02	1.00	−0.34	1.30
NGC 4117	S2	133	44.85	41.51	40.64	−0.31	0.79	−0.86	0.54
NGC 4143	L1.9	18	46.43	42.57	41.27	−0.37	0.72	−1.06	−0.45
NGC 4151	S1.5	22	45.76	43.54	44.07	−0.27	0.84	−0.35	0.60
NGC 4203	L1.9	15	46.01	42.30	41.47	−0.42	0.66	−0.93	−0.11
NGC 4258	S1.9	8	45.71	41.69	41.76	−0.70	0.38	−0.81	0.16
NGC 4261	L2	32	46.83	44.06	42.41	0.02	1.00	−0.91	−0.49
NGC 4278	L1.9	10	47.31	43.11	41.20	−0.35	0.75	−1.25	−1.08
NGC 4374	L2	20	47.31	43.77	41.58	−0.10	0.98	−1.18	−1.00
NGC 4388	S2	18	44.91	42.42	44.00	−0.56	0.51	−0.19	1.19
NGC 4450	L1.9	18	45.41	42.11	41.58	−0.36	0.73	−0.79	0.34
NGC 4486	L2	17	47.59	44.47	41.79	0.13	1.00	−1.19	−1.16
NGC 4501	S2	18	46.01	41.88	41.52	−0.65	0.43	−0.92	−0.10
NGC 4548	L2	18	45.51	41.95	41.03	−0.36	0.73	−0.92	0.15
NGC 4565	S1.9	10	45.81	41.84	40.80	−0.46	0.62	−1.03	−0.11
NGC 4579	S1.9	18	45.96	42.93	42.38	−0.28	0.82	−0.74	0.11
NGC 4594	L2	11	47.15	43.06	41.94	−0.48	0.60	−1.07	−0.82
NGC 4736	L2	5	45.41	40.86	40.86	−0.84	0.28	−0.93	0.19
NGC 5033	S1.5	20	45.41	42.30	42.24	−0.41	0.68	−0.65	0.47
NGC 5194	S2	8	45.01	41.37	41.04	−0.51	0.57	−0.82	0.51
NGC 5252	S2	99	46.23	43.88	44.21	−0.26	0.84	−0.42	0.30
NGC 5347	S2	33	44.81	42.53	41.24	0.09	1.00	−0.73	0.69
NGC 5548	S1.5	75	46.14	43.60	44.79	−0.49	0.58	−0.28	0.48
NGC 5929	S2	36	45.33	43.40	41.94	0.23	1.00	−0.70	0.47
NGC 6166	S2	124	47.30	44.59	41.80	0.27	1.00	−1.13	−0.95
NGC 6251	S2	102	46.84	45.30	43.39	0.44	1.00	−0.71	−0.30
NGC 6500	L2	43	46.39	43.83	41.35	0.25	1.00	−1.03	−0.40

Table 3
(Continued)

Source (1)	Type (2)	D (Mpc) (3)	Log ($L_{\rm Edd}$) (4)	Log (L_j) (5)	Log ($L_{\rm bol}$) (6)	Log $\sqrt{\left(\frac{f(j)}{f_{\rm max}}\right)}$ (7)	j (8)	Log ($B/B_{\rm Edd}$) (9)	Log ($B/10^4$ G) (10)
NGC 7469	S1	71	44.92	43.46	44.55	−0.16	0.94	−0.08	1.29
NGC 7672	S2	57	44.91	42.64	44.61	−0.58	0.50	−0.06	1.31
NGC 7743	S2	26	44.58	42.45	40.95	0.18	1.00	−0.75	0.79
PG 0026+129	Q	672	45.84	44.75	45.68	−0.01	1.00	−0.03	0.87
PG 0052+251	Q	739	46.45	44.21	45.90	−0.51	0.57	−0.11	0.49
PG 0804+761	Q	461	46.39	44.20	45.50	−0.41	0.67	−0.18	0.45
PG 0844+349	Q	287	45.45	43.27	44.53	−0.40	0.68	−0.19	0.91
PG 0953+414	Q	1198	46.37	44.73	45.74	−0.19	0.91	−0.13	0.51
PG 1211+143	Q	388	45.72	45.41	44.85	0.52	1.00	−0.18	0.79
PG 1226+023	Q	755	46.85	47.55	46.94	0.83	1.00	0.02	0.42
PG 1229+204	Q	287	45.99	43.51	45.53	−0.65	0.43	−0.10	0.74
PG 1307+085	Q	739	46.55	43.89	45.75	−0.67	0.41	−0.17	0.39
PG 1411+442	Q	407	46.01	43.69	44.77	−0.41	0.68	−0.26	0.57
PG 1426+015	Q	392	46.78	43.89	45.13	−0.61	0.47	−0.34	0.10
PG 1613+658	Q	605	46.49	44.45	45.58	−0.34	0.76	−0.19	0.40
PG 2130+099	Q	273	46.27	43.82	44.79	−0.42	0.66	−0.30	0.39
3C 120	S1	148	45.84	45.75	45.19	0.59	1.00	−0.13	0.78
3C 390.3	S1	258	46.64	45.42	45.24	0.18	1.00	−0.29	0.22
Sgr A^*		0.008	44.71	39.19	34.52	−0.17	0.93	−2.09	−0.61

Notes. All luminosities are in erg s^{-1}.

(This table is available in its entirety in machine-readable form.)

Figure 12, histograms of spin values are shown in Figure 14, and values are listed in Tables 1–5.

The accretion disk magnetic field strength in physical units is obtained using Equation (8) and is illustrated in Figure 12. It is easy to see that the accretion disk magnetic field strengths for AGNs are quite similar for all AGN types and have a broad range of values with a peak at about 10^4 G. The accretion disk magnetic field strengths for the GBH measurements are all quite similar and have values of about 10^8 G, with the exception of the one measurement of AO 6200 and one measurement of V404 Cyg. Histograms of the accretion disk magnetic field strength in physical units for each sample are shown in Figure 13, and the values are summarized in Table 1.

Histograms of the black hole spin are shown in Figure 14 and summarized in Table 1. As noted earlier, spin values of sources with spin functions greater than 1 indicate a spin value of 1, as is evident in Figure 14, and some of the spin distributions are clearly asymmetric.

5. Discussion

Three key results are presented in Section 4 related to black hole spin: (1) Black hole spin functions and spin values obtained for all source types studied are relatively high. For the NB16, D16, and S15 samples, the mean spin values are about 0.9, and for the M03 sample the mean spin value is about 0.8 (see Table 1). As noted earlier, the spin distributions become skewed when $\sqrt{f(j)/f_{\rm max}} > 1$, since in this case the spin is set equal to 1, so the mean value of the spin (listed in Table 1) is smaller than that indicated by the mean value of the spin function. (2) All of the source types studied, including LINERs (NB16), FR II sources (D16), GBHs (S15), and a compilation of compact radio sources (M03), have similar values of the spin function $\sqrt{(f(j)/f_{\rm max})}$ and black hole spin j. This suggests that AGN type is not determined by black hole spin for the types of sources studied here. This is consistent with the finding of D16, that subtypes of FR II sources including HEGs, RLQs, and LEGs have similar spin functions and spin values, and thus their AGN type is not determined by black hole spin. (3) For the GBHs with numerous measurements per source, the dispersions of the spin indicators, including the spin function and spin value, are smaller than those of the magnetic field strengths. The implications of these results will be discussed below.

Three key results are presented in Section 4 related to accretion disk magnetic field strengths: (1) There is a range of mean values of the Eddington-normalized magnetic field strengths, and these are related to source type. This is not surprising since for AGNs some source types are related to ($L_{\rm bol}/L_{\rm Edd}$) (e.g., Ho 2009). (2) The distributions of accretion disk magnetic field strengths in physical units are broad and similar for the AGN samples studied and peak at about 10^4 G. Thus, the accretion disk magnetic field strength in physical units is not related to AGN type. The field strength distributions for the GBHs are similar for most of the measurements and peak at about 10^8 G, with the exception of the one measurement of AO 6200 and one measurement of V404 Cyg. (3) The dispersion of the magnetic field strengths, both in Eddington units and in physical units, is larger than that of the spin indicators for the GBH sample and for the two individual GBHs with numerous observations per source.

Point (3) from each paragraph above can be understood in the following way. Over the course of the numerous simultaneous radio and X-ray observations of the GBHs, the spin of the black hole remains constant, but the accretion disk magnetic field strength varies with the accretion rate. This leads to the field strengths having a larger dispersion than the spin

Table 4
Beam Power, Spin Parameters, and Disk Magnetic Field Strength Estimates for 100 FR II AGNs, Including the 97 D16 Sources plus 3 W Sources from Grimes et al. (2004)

Source (1)	Type (2)	z (3)	Log $(L_{\rm Edd})$ (4)	Log (L_j) (5)	Log $(L_{\rm bol})$ (6)	Log $\left(\sqrt{\frac{f(j)}{f_{\rm max}}}\right)$ (7)	j (8)	Log $(B/B_{\rm Edd})$ (9)	Log $(B/10^4\ {\rm G})$ (10)
3C 33	HEG	0.059	46.68	44.39	45.63	−0.42	0.67	−0.23	0.27
3C 192	HEG	0.059	46.52	44.05	45.22	−0.45	0.63	−0.29	0.29
3C 285	HEG	0.079	46.64	44.04	44.36	−0.30	0.80	−0.50	0.01
3C 452	HEG	0.081	46.83	44.62	45.08	−0.22	0.88	−0.38	0.04
3C 388	HEG	0.09	46.95	44.42	44.13	−0.15	0.94	−0.62	−0.26
3C 321	HEG	0.096	46.90	44.24	45.79	−0.59	0.48	−0.24	0.14
3C 433	HEG	0.101	47.08	44.80	44.38	−0.05	0.99	−0.59	−0.30
3C 20	HEG	0.174	46.69	45.11	44.75	0.14	1.00	−0.43	0.06
3C 28	HEG	0.195	46.99	44.88	45.51	−0.23	0.87	−0.32	0.02
3C 349	HEG	0.205	46.67	44.83	45.10	−0.08	0.98	−0.35	0.15
3C 436	HEG	0.214	46.97	44.97	45.20	−0.11	0.97	−0.39	−0.03
3C 171	HEG	0.238	46.71	45.09	46.19	−0.19	0.91	−0.11	0.37
3C 284	HEG	0.239	47.01	44.91	45.88	−0.30	0.80	−0.25	0.09
3C 300	HEG	0.27	46.67	45.16	45.86	−0.08	0.98	−0.18	0.32
3C 438	HEG	0.29	47.22	45.55	45.14	0.12	1.00	−0.46	−0.23
3C 299	HEG	0.367	46.69	45.24	46.50	−0.18	0.92	−0.04	0.45
3C 42	HEG	0.395	47.06	45.32	45.58	−0.05	0.99	−0.32	−0.02
3C 16	HEG	0.405	46.77	45.34	45.50	0.06	1.00	−0.28	0.17
3C 274.1	HEG	0.422	47.05	45.50	44.90	0.20	1.00	−0.47	−0.16
3C 244.1	HEG	0.428	47.09	45.13	46.57	−0.37	0.73	−0.11	0.17
3C 457	HEG	0.428	46.92	45.45	46.03	−0.04	1.00	−0.19	0.18
3C 46	HEG	0.437	47.30	45.39	46.34	−0.24	0.86	−0.21	−0.03
3C 341	HEG	0.448	47.13	45.40	46.34	−0.19	0.91	−0.17	0.10
3C 172	HEG	0.519	47.00	45.49	46.62	−0.17	0.92	−0.08	0.25
3C 330	HEG	0.549	47.22	45.90	47.11	−0.14	0.95	−0.02	0.20
3C 49	HEG	0.621	47.22	45.62	46.33	−0.11	0.97	−0.20	0.03
3C 337	HEG	0.635	47.07	45.31	45.30	0.01	1.00	−0.39	−0.09
3C 34	HEG	0.69	47.33	45.81	47.60	−0.32	0.78	0.06	0.23
3C 441	HEG	0.708	47.36	45.81	46.22	−0.02	1.00	−0.25	−0.09
3C 247	HEG	0.749	47.52	45.54	46.90	−0.36	0.74	−0.14	−0.06
3C 277.2	HEG	0.766	47.15	45.93	47.13	−0.11	0.97	0.00	0.26
3C 340	HEG	0.775	47.15	45.82	46.50	−0.03	1.00	−0.14	0.12
3C 352	HEG	0.806	47.31	45.92	47.20	−0.17	0.93	−0.02	0.16
3C 263.1	HEG	0.824	47.38	46.11	46.85	−0.02	1.00	−0.12	0.03
3C 217	HEG	0.897	46.93	45.99	46.81	0.05	1.00	−0.03	0.34
3C 175.1	HEG	0.92	47.20	46.05	46.50	0.08	1.00	−0.15	0.08
3C 289	HEG	0.967	47.54	45.93	46.00	0.03	1.00	−0.34	−0.27
3C 280	HEG	0.996	47.55	45.73	47.68	−0.44	0.64	0.03	0.09
3C 356	HEG	1.079	47.56	46.40	46.82	0.08	1.00	−0.16	−0.11
3C 252	HEG	1.103	47.41	46.23	47.15	−0.04	1.00	−0.06	0.07
3C 368	HEG	1.132	47.56	46.39	47.22	−0.01	1.00	−0.07	−0.02
3C 267	HEG	1.14	47.50	46.28	46.93	0.01	1.00	−0.13	−0.04
3C 324	HEG	1.206	47.68	46.19	47.10	−0.12	0.96	−0.13	−0.13
3C 266	HEG	1.275	47.49	46.35	47.54	−0.08	0.98	0.01	0.11
3C 13	HEG	1.351	47.71	46.41	47.23	−0.05	0.99	−0.11	−0.13
4C 13.66	HEG	1.45	47.31	46.41	47.17	0.08	1.00	−0.03	0.15
3C 437	HEG	1.48	47.50	46.85	46.90	0.31	1.00	−0.13	−0.04
3C 241	HEG	1.617	47.68	46.57	47.29	0.03	1.00	−0.09	−0.09
3C 470	HEG	1.653	47.56	46.47	46.47	0.19	1.00	−0.24	−0.18
3C 322	HEG	1.681	47.62	46.71	46.51	0.29	1.00	−0.24	−0.22
3C 239	HEG	1.781	47.68	46.68	46.92	0.17	1.00	−0.17	−0.17
3C 294	HEG	1.786	47.57	46.65	47.51	0.05	1.00	−0.01	0.04
3C 225*B*	HEG	0.582	47.11	45.88	46.44	0.03	1.00	−0.15	0.13
3C 55	HEG	0.735	47.27	46.25	46.12	0.24	1.00	−0.25	−0.05
3C 68.2	HEG	1.575	47.65	46.32	47.09	−0.04	0.99	−0.12	−0.12
3C 35	LEG	0.067	46.76	43.89	43.65	−0.25	0.85	−0.68	−0.23
3C 326	LEG	0.088	46.50	44.34	44.28	−0.09	0.98	−0.49	0.10
3C 236	LEG	0.099	46.93	44.28	44.11	−0.20	0.90	−0.62	−0.25
4C 12.03	LEG	0.156	46.97	44.51	44.51	−0.19	0.91	−0.54	−0.19
3C 319	LEG	0.192	46.44	44.83	44.59	0.10	1.00	−0.41	0.21

Table 4
(Continued)

Source (1)	Type (2)	z (3)	Log ($L_{\rm Edd}$) (4)	Log (L_j) (5)	Log ($L_{\rm bol}$) (6)	Log $\left(\sqrt{\frac{f(j)}{f_{\rm max}}}\right)$ (7)	j (8)	Log ($B/B_{\rm Edd}$) (9)	Log ($B/10^4$ G) (10)
3C 132	LEG	0.214	46.85	44.86	45.39	−0.17	0.92	−0.32	0.09
3C 123	LEG	0.218	46.93	45.83	45.26	0.31	1.00	−0.37	0.00
3C 153	LEG	0.277	47.05	45.11	45.86	−0.21	0.89	−0.26	0.05
4C 14.27	LEG	0.392	46.84	45.30	45.46	0.03	1.00	−0.30	0.11
3C 200	LEG	0.458	47.06	45.43	46.03	−0.09	0.98	−0.22	0.08
3C 295	LEG	0.461	47.57	46.13	45.53	0.23	1.00	−0.45	−0.40
3C 19	LEG	0.482	47.27	45.47	46.07	−0.14	0.95	−0.26	−0.06
3C 427.1	LEG	0.572	47.27	45.50	46.61	−0.24	0.86	−0.15	0.05
3C 249.1	Q	0.311	47.41	45.09	46.92	−0.56	0.52	−0.11	0.02
3C 351	Q	0.371	47.61	45.31	46.38	−0.38	0.71	−0.27	−0.24
3C 215	Q	0.411	46.41	45.37	46.13	0.04	1.00	−0.06	0.57
3C 47	Q	0.425	47.31	45.69	46.82	−0.20	0.90	−0.11	0.07
3C 334	Q	0.555	47.81	45.79	46.91	−0.31	0.79	−0.20	−0.27
3C 275.1	Q	0.557	46.41	44.94	46.50	−0.26	0.85	0.02	0.65
3C 263	Q	0.646	47.21	45.83	47.25	−0.20	0.90	0.01	0.24
3C 207	Q	0.684	46.61	45.85	46.59	0.12	1.00	0.00	0.52
3C 254	Q	0.734	47.41	45.80	47.25	−0.27	0.83	−0.04	0.09
3C 175	Q	0.768	48.01	46.11	46.64	−0.15	0.94	−0.30	−0.47
3C 196	Q	0.871	47.71	46.62	46.62	0.19	1.00	−0.24	−0.26
3C 309.1	Q	0.904	47.21	46.19	47.24	−0.02	1.00	0.01	0.23
3C 336	Q	0.927	47.31	46.01	47.00	−0.08	0.98	−0.07	0.11
3C 245	Q	1.029	47.51	46.20	47.05	−0.06	0.99	−0.10	−0.02
3C 212	Q	1.049	47.31	46.27	47.02	0.04	1.00	−0.06	0.11
3C 186	Q	1.063	47.61	46.31	47.38	−0.10	0.97	−0.05	−0.02
3C 208	Q	1.11	47.51	46.36	47.00	0.04	1.00	−0.11	−0.03
3C 204	Q	1.112	47.61	46.23	46.74	0.00	1.00	−0.19	−0.16
3C 190	Q	1.197	46.81	46.38	47.21	0.20	1.00	0.09	0.52
3C 68.1	Q	1.238	48.01	46.61	46.85	0.05	1.00	−0.26	−0.43
4C 16.49	Q	1.296	47.91	46.34	46.86	−0.05	0.99	−0.23	−0.35
3C 181	Q	1.382	47.71	46.52	47.91	−0.14	0.95	0.04	0.02
3C 268.4	Q	1.4	47.91	46.92	47.79	0.03	1.00	−0.03	−0.15
3C 14	Q	1.469	47.51	46.39	47.42	−0.04	0.99	−0.02	0.06
3C 270.1	Q	1.519	47.11	46.90	47.05	0.41	1.00	−0.01	0.26
3C 205	Q	1.534	47.71	46.52	47.54	−0.06	0.99	−0.04	−0.06
3C 432	Q	1.805	48.21	46.65	47.22	−0.07	0.99	−0.22	−0.49
3C 191	Q	1.956	47.81	46.78	47.75	−0.01	1.00	−0.01	−0.09
3C 9	Q	2.012	47.91	46.97	47.39	0.14	1.00	−0.11	−0.24
3C 223	W	0.136	46.59	44.54	45.82	−0.35	0.74	−0.17	0.37
3C 79	W	0.255	46.90	45.31	46.13	−0.12	0.96	−0.17	0.22
3C 109	W	0.305	46.41	45.33	46.86	−0.14	0.95	0.10	0.73

Notes. All luminosities are in erg s^{-1}.

(This table is available in its entirety in machine-readable form.)

indicators. The variation of the accretion disk magnetic field strength impacts the beam power of the outflow, since the beam power is regulated in part by the magnetic field strength of the disk, but it does not impact the black hole spin. The fact that there are numerous simultaneous radio and X-ray observations for the GBHs allow the changes in the accretion rate and resulting changes in the beam power to be studied.

Black hole spins obtained here can be compared with those obtained independently. GX 339−4 has published spin values of 0.94 ± 0.02 (Miller et al. 2009) and $0.95^{+0.03}_{-0.05}$ (García et al. 2015), and the value obtained here is 0.92 ± 0.06 (see Table 1). Thus, the value obtained here is in good agreement with that indicated by a well-established and independent method. For AGNs there is good agreement between the spin values obtained here and those obtained with the X-ray reflection method (see Table 1). The spin values obtained with the X-ray reflection method are from Patrick et al. (2012), Walton et al. (2013), and the compilation of Vasudevan et al. (2016). Only AGNs with X-ray reflection spin measurements described by Reynolds (2019) as being "robust" were compared with spin determination obtained here. The uncertainties of the spin values for individual AGNs are estimated as described in Section 3.3.

The value of the spin for AO 6200 obtained here is relatively high. Gou et al. (2010) used a single high-quality X-ray spectrum from 1975 and obtained a low value for the spin of this source by fitting the spectrum with a detailed model of the accretion disk. The X-ray data suggest a value of

Table 5
Beam Power, Spin Parameters, and Disk Magnetic Field Strength Estimates for 576 LINERs

Source NB (1)	z (2)	Log $(L_{\rm Edd})$ (3)	Log (L_j) (4)	Log $(L_{\rm bol})$ (5)	Log $\left(\sqrt{\frac{f(j)}{f_{\rm max}}}\right)$ (6)	j (7)	Log $(B/B_{\rm Edd})$ (8)	Log $(B/10^4$ G) (9)
1	0.0608	45.67	43.16	42.97	−0.17	0.93	−0.58	0.42
2	0.1117	46.39	44.55	44.80	−0.08	0.98	−0.34	0.30
3	0.1628	45.95	43.66	43.51	−0.12	0.96	−0.53	0.33
4	0.1316	46.63	43.51	43.09	−0.30	0.81	−0.76	−0.24
5	0.1319	45.56	43.51	42.47	0.14	0.95	−0.67	0.39

Notes. All luminosities are in erg s^{-1}.

(This table is available in its entirety in machine-readable form.)

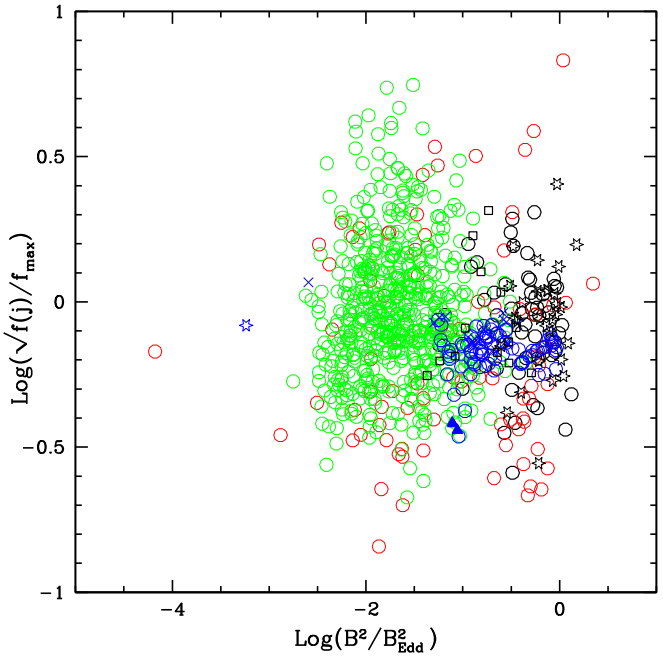

Figure 8. Square root of the black hole spin function vs. the square of the accretion disk magnetic field strength in Eddington units. Here and throughout the paper: the 576 LINERs from NB16 are shown as green cirlces; the 97 FR II sources from D16 are shown in black (circles represent 55 high-excitation radio galaxies, stars represent 29 radio-loud quasars, and squares represent 13 low-excitation radio galaxies); the 80 compact radio sources from M03 are shown as red circles, and the 102 GBHs from S15 are shown in blue (open circles represent GX 339−4, crosses represent V404 Cyg, solid triangles represent XTE J1118+480, and an open star represents AO 6200). Values of $g_{\rm bol} = 1$ and $g_j = 0.1$ have been adopted for all sources. The source with a value of $\mathrm{Log}(B^2/B^2_{\rm Edd}) \simeq -4$ is Sgr A^*. Fits show that there is no covariance between the quantities $\mathrm{Log}(\sqrt{f(j)/f_{\rm max}})$ and $\mathrm{Log}(B/B_{\rm Edd})^2$.

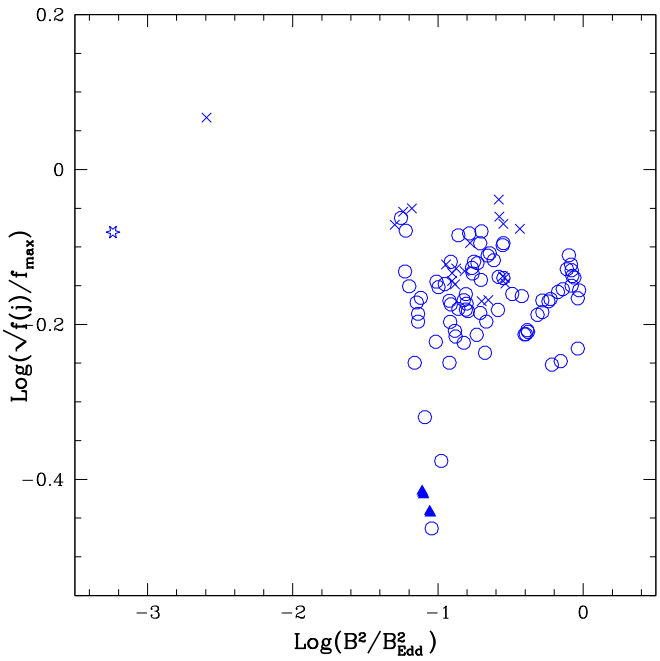

Figure 9. Same as Figure 8, but with only results for GBHs shown. There are 76 measurements for the source GX 339−4 shown as open circles, 20 measurements for the source V404 Cyg shown as crosses, 5 measurements for the source XTE J1118+480 shown as solid triangles, and 1 measurement for the source AO 6200 shown as an open star (a second observation of AO 6200 is discussed in Section 5).

$L_{\rm bol}/L_{\rm Edd} \simeq 0.11$ (Gou et al. 2010). Kuulkers et al. (1999) report radio observations obtained at about the same time as the X-ray outburst. We consider the 1.4 GHz data point with a flux density of about 0.3 Jy obtained by Owen et al. (1976) and listed in Table 1 of Kuulkers et al. (1999) because it is comparable in frequency to the FP constructed by NB16, to which all of the compact radio sources studied here are scaled. Converting this flux density to a flux by multiplying by 1.4 GHz, and using the distance to the source provided by Gou et al. (2010), a value of $\mathrm{Log}(L_j) \simeq 37.23$ is obtained from the radio luminosity of $\mathrm{Log}(L_R) \simeq 29.74$ using the values of C and D from Table 1 of D18 following the procedure used for all of the GBHs discussed here and in D18. A value of $\mathrm{Log}(B/B_{\rm Edd}) \simeq -0.23$ is indicated by $L_{\rm bol}/L_{\rm Edd} \simeq 0.11$, obtained with Equation (7) for $A \simeq 0.47$ applicable for GBHs (D18). Combining the value of $\mathrm{Log}(L_j) \simeq 37.23$ with the value of $L_{\rm Edd}$ listed in Table 2 to obtain $L_j/L_{\rm Edd}$, and assuming the standard values of $g_{\rm bol} = 1$ and $g_j = 0.1$, a value of $\mathrm{Log}\sqrt{(f(j)/f_{\rm max})} \simeq -0.11$ is obtained with Equation (2), and a spin of about 0.97 is obtained with Equation (9). Interestingly, this is similar to the spin value of 0.98 obtained here (see Table 1). Note that the field strength listed in Table 2 is significantly different, $\mathrm{Log}(B/B_{\rm Edd}) \simeq -1.62$. Thus, even though this field strength is significantly lower than that indicated during the outburst, the combination of contemporaneously obtained radio and X-ray data yields a value of the spin that is consistent. Thus, the empirical results indicate that the magnetic field strength of the accretion disk is variable, but the spin of the black hole remains roughly constant, as expected

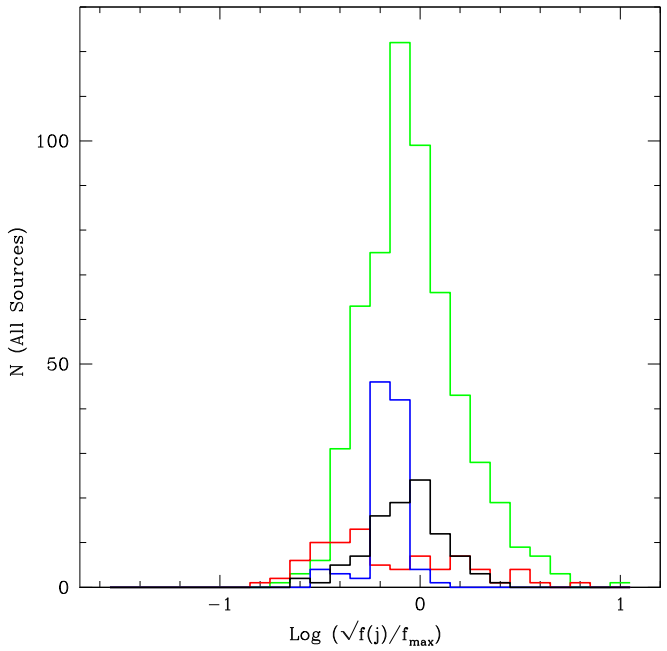

Figure 10. Histograms of the square root of the spin function shown in Figure 8 for each of the four samples considered. As in all of the figures, the 576 LINERs from NB16 are shown in green, the 97 FR II sources from D16 are shown in black, the 80 compact radio sources from M03 are shown in red, and the 102 GBHs from S15 are shown in blue. The results are summarized in Table 1.

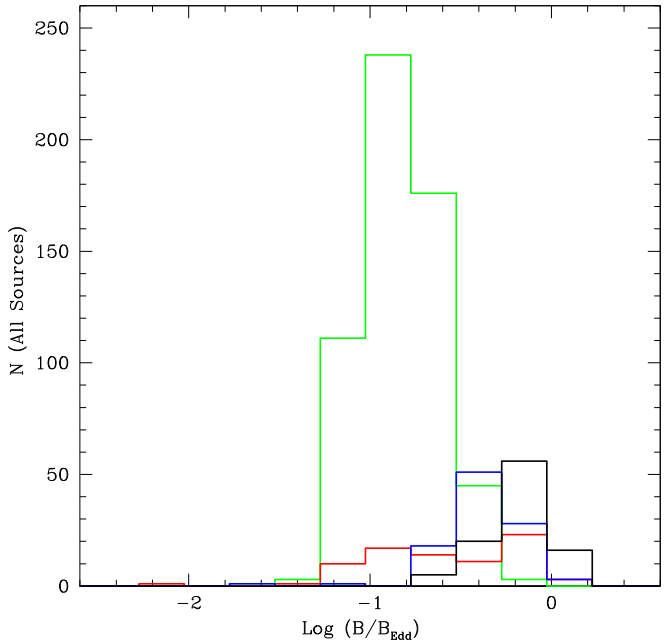

Figure 11. Histograms of the Eddington-normalized accretion disk magnetic field strengths shown in Figure 8 for each of the four samples considered. The colors are as in Figure 1, and the results are summarized in Table 1.

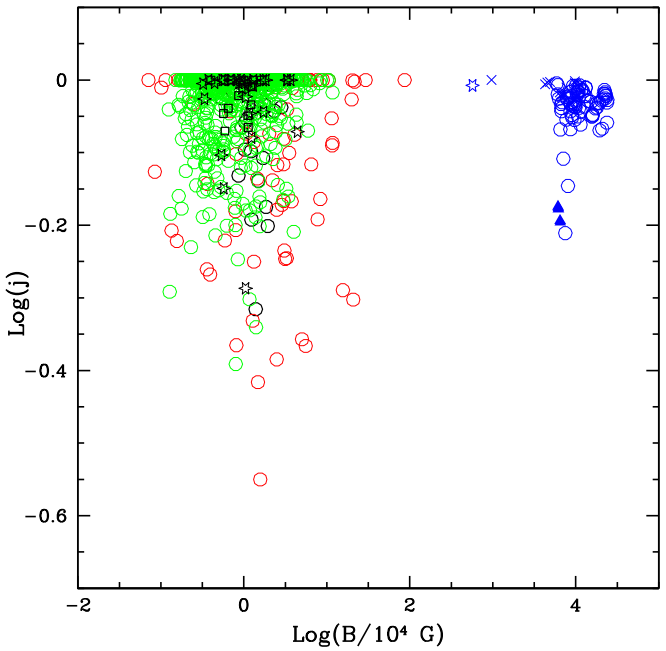

Figure 12. Black hole spin vs. the accretion disk magnetic field strength in units of 10^4 G. The black hole spin is obtained from the spin function as described in the text. When the spin function $f(j)/f_{\rm max} \geqslant 1$, the spin j is set equal to 1. The symbols are as in Figure 8.

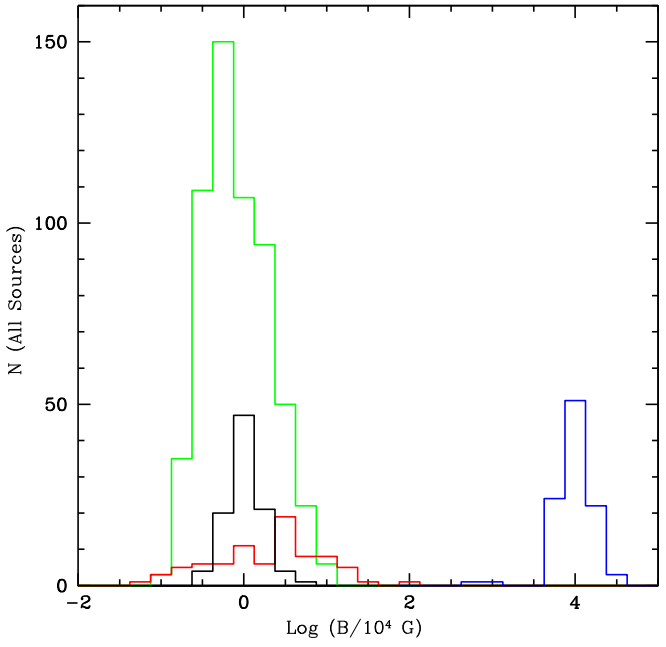

Figure 13. Histograms of the accretion disk magnetic field strengths shown in Figure 12 for each of the four samples considered. The colors are as in Figure 1, and the results are summarized in Table 1.

in the context of the outflow-based method applied here (e.g., Equation (6)).

Accretion disk magnetic field strengths have been estimated for GBHs in the context of an outflow model for these systems by Piotrovich et al. (2015b), who report values of $\sim 10^8$ G for these systems. Accretion disk magnetic field strengths have been estimated for AGNs in the context of a detailed accretion disk model, and values of $\sim 10^4$ G are reported (e.g., Mikhailov et al. 2015; Piotrovich et al. 2015a). Thus, the accretion disk magnetic field strengths obtained here for GBHs and AGNs are similar to values indicated by other methods.

Dispersions of the distributions of empirically determined quantities for each of the samples listed in Table 1 can be compared with the uncertainty per source estimated based on the uncertainties of the input parameters, as discussed in Sections 2

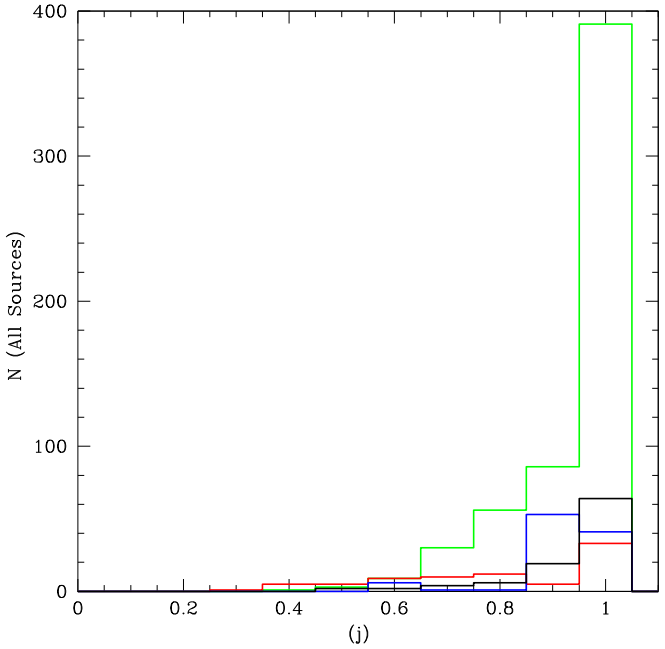

Figure 14. Histograms of spin values for each of the four samples shown in Figure 12. The colors are as in Figure 1. The results are summarized in Table 1.

and 3.3. The dispersions of the full population are significantly larger than the measurement uncertainty per source divided by the square root of the number of sources per sample. Thus, the results are consistent with the sources having a broad distribution of each of the quantities studied here.

6. Summary

The "outflow method" of determining black hole spin functions and spins proposed and applied to a sample of FR II sources by D16 is applied to the samples studied by D18. This requires a value of the outflow beam power L_j for each source. Beam powers are obtained for FP sources using the method proposed and applied by D18 and explained in Section 1.1, and values for the FR II sources are obtained using the strong shock method. Values of $L_{\rm bol}$ and $L_{\rm Edd}$ are obtained using standard methods. Equation (2) is used to solve for the spin function using the best-fit values of A obtained by D18 (see Table 2 of that paper). As explained in Section 3, assuming that the outflows of each source are powered at least in part by the spin of the black hole, it is shown that Equation (2) can be applied to FP sources. The same sets of equations used to obtain Equation (2) may be manipulated to solve for the accretion disk magnetic field strength, resulting in Equations (7) and (8). The accretion disk magnetic field strengths are independent of the beam power. A more intuitive derivation of the key equations is provided in Section 3.2; here the empirical nature of the method is explicitly demonstrated.

In the context of the outflow method, black hole spin indicators and indicators of the accretion disk properties are obtained without specifying an accretion disk emission model and without specifying a model relating beam power to compact radio source luminosity. Thus, the accretion disk magnetic field strengths obtained may be used to study and constrain accretion disk emission models, and the empirically determined relationship between beam power and compact radio luminosity may be used to study and constrain jet-launching and emission models, as discussed in Section 3.3. In addition, the dimensionless field strength provides an estimate of the mass accretion rate, as discussed in Sections 3.1 and 3.3.

The GBH sample of S15 and the AGN samples of M03, NB16, and D16 are used to obtain spin functions, spin values, and magnetic field strengths for each measurement of the beam power, bolometric disk luminosity, and black hole mass. This requires that values of the normalization factors $g_{\rm bol}$ and g_j be specified. Figure 1 in D18 suggests values of $g_{\rm bol} = 1$ and $g_j = 0.1$, and these values are adopted here. Tables 2–5 list all quantities of interest, and spin indicators and accretion disk magnetic field strengths are summarized in Table 1.

Reliable and independent spin determinations are available for one GBH and six AGNs, and there is good agreement between values obtained here and published values; the comparisons are listed in Table 1. The remaining spin values obtained here could be considered predictions and indicate relatively high values for M87 and Sgr A^* (see Table 1); values for all sources are included in Tables 2–5. There are several factors that could affect these values, such as those discussed in Sections 1.1, 4, and 5.

The spin values obtained are similar for all types of AGNs studied and for the GBHs studied, suggesting that spin value does not determine AGN type for the types of sources studied here. The distributions of accretion disk magnetic field strengths in physical units for the AGNs are broad and similar for different AGN types and peak at a value of about 10^4 G; those for GBHs have distibutions that peak at a value of about 10^8 G.

Multiple measurements of a particular source provide a unique opportunity to study and test the outflow method of determining source parameters. The GBHs studied here allow the use of simultaneous or contemporaneous radio and X-ray data to study the accretion disk magnetic field strength and black hole spin of one source at different times. The empirical determinations indicate that the variation of the disk field strength modifies the beam power but does not affect the empirically determined black hole spin. The fact that contemporaneous radio and X-ray data yield a fixed spin but a variable field strength provides support for the method and suggests that it provides an accurate description of the types of sources studied here.

The spin values obtained here are relatively high, with typical spin values ranging from about 0.6 to 1. This could be a selection effect, since all of the sources studied have powerful collimated outflows, and sources with low spin may produce weak outflows. There is a hint of this in the current analysis. Considering the AGN samples, the spin values of the M03 sources extend to lower values than those for NB16 and D16, and the M03 sample includes many lower-luminosity radio sources. In addition, in the context of the models considered here, an outflow requires both an accretion event to provide the magnetized plasma and field to thread the ergosphere of the black hole and a spinning black hole to provide an energy source to power the outflow.

It is a pleasure to thank the many colleagues with whom this work was discussed, especially Rychard Bouwens, Jean Brodie, Ray Carlberg, Martin Haehnelt, Zoltan Haiman, Garth Illingworth, Massimo Ricotti, Michele Trenti, and Rosie Wyse. Thanks are extended to Chris Reynolds and to the referee for providing very helpful comments and suggestions. This work was supported in part by Penn State University and performed in part at the Aspen Center for Physics, which is supported by National Science Foundation grant PHY-1607611.

ORCID iDs

Ruth A. Daly https://orcid.org/0000-0002-5503-0691

References

Abbott, et al. The LIGO Scientific Collaboration, the Virgo Collaboration 2018, arXiv:1811.12940
Balbus, S. A., & Hawley, J. F. 1991, ApJ, 376, 214
Balbus, S. A., & Hawley, J. F. 1998, RvMP, 70, 1
Begelman, M. C., Blandford, R. D., & Rees, M. J. 1984, RvMp, 56, 255
Bentz, M. C., Denney, K. D., Cackett, E. M., et al. 2006, ApJ, 651, 775
Blandford, R. D. 1990, in Active Galactic Nuclei, ed. T. J. L. Courvoisier & M. Mayor (Berlin: Springer), 161
Blandford, R. D., Meier, D. L., & Readhead, A. 2019, ARA&A, 57, 467
Blandford, R. D., & Payne, D. G. 1982, MNRAS, 199, 883
Blandford, R. D., & Znajek, R. L. 1977, MNRAS, 179, 433
Bonchi, A., La Franca, F., Melini, G., Bongiorno, A., & Fiore, F. 2013, MNRAS, 429, 1970
Cantrell, A. G., Bailyn, C. D., Orosz, J. A., et al. 2010, ApJ, 710, 1127
Corbel, S., Coriat, M., Brocksopp, C., et al. 2013, MNRAS, 428, 2500
Corbel, S., Körding, E., & Kaaret, P. 2008, MNRAS, 389, 1697
Corbel, S., Nowak, M. A., Fender, R. P., Tzioumis, A. K., & Markoff, S. 2003, A&A, 400, 1007
Croston, J. H., Birkinshaw, M., Hardcastle, M. J., & Worrall, D. M. 2004, MNRAS, 353, 879
Croston, J. H., Hardcastle, M. J., Harris, D. R., et al. 2005, ApJ, 626, 733
Daly, R. A. 1994, ApJ, 426, 38
Daly, R. A. 2009a, ApJL, 691, L72
Daly, R. A. 2009b, ApJL, 696, L32
Daly, R. A. 2011, MNRAS, 414, 1253
Daly, R. A. 2016, MNRAS, 458, L24
Daly, R. A., Djorgovski, S. G., Freeman, K. A., et al. 2008, ApJ, 677, 1
Daly, R. A., Kharb, P., O'Dea, C. P., et al. 2010, ApJS, 187, 1
Daly, R. A., & Sprinkle, T. B. 2014, MNRAS, 438, 3233
Daly, R. A., Sprinkle, T. B., O'Dea, C. P., Kharb, P., & Baum, S. A. 2012, MNRAS, 423, 2498
Daly, R. A., Stout, D. A., & Mysliwiec, J. N. 2018, ApJ, 863, 117
Dermer, C., Finke, J., & Menon, G. 2008, Black-Hole Engine Kinematics, Flares from PKS2155-304, and Multiwavelength Blazar Analysis (Trieste: SISSA)
Dicken, D., Tadhunter, C., Morganti, R., et al. 2014, ApJ, 788, 98
Fabian, A. C., Rees, M. J., Stella, L., & White, N. E. 1989, MNRAS, 238, 729
Falcke, H., Körding, E., & Markoff, S. 2004, A&A, 414, 895
Fanaroff, B. L., & Riley, J. M. 1974, MNRAS, 164, 31
Fazeli, N., Busch, G., Valencia-S, M., et al. 2019, A&A, 622, 128
Ferrarese, L. 2002, in Proc. II KIAS Astrophys. Workshop, Current High Energy Emission around Black Holes, ed. C.-H. Lee & H.-Y. Chang (Singapore: World Scientific), 3
Ferrarese, L., & Merritt, D. 2000, ApJL, 539, L9
Gallo, E., Fender, R. P., Miller-Jones, J. C. A., et al. 2006, MNRAS, 370, 1351
Gallo, E., Fender, R. P., & Pooley, G. G. 2003, MNRAS, 344, 60
García, J. A., Steiner, J. F., McClintock, J. E., et al. 2015, ApJ, 813, 84
Ghez, A. M., Salim, S., Weinberg, N. N., et al. 2008, ApJ, 689, 1044
Gnedin, Yu. N., Afanasiev, V. L., Borisov, N. V., et al. 2012, ARep, 56, 573
Godfrey, L. E. H., & Shabala, S. S. 2013, ApJ, 767, 12
Gou, L., McClintock, J. E., Steiner, J. F., et al. 2010, ApJL, 718, L122
Grier, C. J., Pancoast, A., Barth, A. J., et al. 2017, ApJ, 849, 146
Grimes, J. A., Rawlings, S., & Willott, C. J. 2004, MNRAS, 349, 503
Gültekin, K., Cackett, E. M., Miller, J. M., et al. 2009, ApJ, 706, 404
Harwood, J. J., Croston, J. H., Intema, H. T., et al. 2016, MNRAS, 458, 4443
Hawley, J. F., & Balbus, S. A. 1991, ApJ, 376, 223
Heckman, T. M., Kauffmann, G., Brinchmann, J., et al. 2004, ApJ, 613, 109
Heinz, S. 2004, MNRAS, 355, 835
Heinz, S., & Sunyaev, R. A. 2003, MNRAS, 343, L59
Ho, L. C. 2009, ApJ, 699, 626
Ilic, D., Shapovalova, A. I., Popović, L. Č., et al. 2017, FrASS, 4, 12
Khargharia, J., Froning, C. S., Robinson, E. L., & Gelino, D. M. 2013, AJ, 145, 21
King, A. L., Miller, J. M., Gultekin, K., et al. 2013, ApJ, 771, 1
Körding, E. G., Falcke, H., & Corbel, S. 2006a, A&A, 456, 439
Körding, E. G., Fender, R. P., & Migliari, S. 2006b, MNRAS, 369, 1451
Kuulkers, E., Fender, R. P., Spencer, R. E., Davis, R. J., & Morison, I. 1999, MNRAS, 306, 919
Leahy, J. P., Muxlow, T. W. B., & Stephens, P. W. 1989, MNRAS, 239, 401
Leahy, J. P., & Williams, A. G. 1984, MNRAS, 210, 929
Li, Z., Wu, X. B., & Wang, R. 2008, ApJ, 688, 826
McConnell, N. J., & Ma, C. 2013, ApJ, 764, 184
McLure, R. J., Jarvis, M. J., Targett, T. A., Dunlop, J. S., & Best, P. N. 2006, MNRAS, 368, 1395
McLure, R. J., Willott, C. J., Jarvis, M. J., et al. 2004, MNRAS, 351, 347
Meier, D. L. 1999, ApJ, 522, 753
Meier, D. L. 2001, ApJL, 548, L9
Merloni, A., Heinz, S., & di Matteo, T. 2003, MNRAS, 345, 1057
Mikhailov, A. G., & Gnedin, Y. N. 2018, ARep, 62, 1
Mikhailov, A. G., Gnedin, Y. N., & Belonovsky, A. V. 2015, Ap, 58, 157
Miller, J. M., Reynolds, C. S., Fabian, A. C., Miniutti, G., & Gallo, L. C. 2009, ApJ, 697, 900
Nisbet, D. M., & Best, P. N. 2016, MNRAS, 455, 2551
O'Dea, C. P., Daly, R. A., Freeman, K. A., Kharb, P., & Baum, S. 2009, A&A, 494, 471
Owen, F. N., Balonek, T. J., Dickey, J., Terzian, Y., & Gottesman, S. T. 1976, ApJL, 203, L15
Patrick, A. R., Reeves, J. N., Porquet, D., et al. 2012, MNRAS, 426, 2522
Penrose, R. 1969, NCimR, 1, 252
Penrose, R., & Floyd, R. M. 1971, NPhS, 229, 177
Piotrovich, M. Y., Buliga, S. D., Gnedin, Y. N., Natsvlishvili, T. M., & Silant'ev, N. A. 2015a, Ap&SS, 357, 99
Piotrovich, M. Y., Gnedin, Y. N., Buliga, S. D., et al. 2015b, in ASP Conf. Ser. 494, Physics and Evolution of Magnetic and Related Stars, ed. Y. Y. Balega, I. I. Romanyuk, & D. O. Kudryavstev (San Francisco, CA: ASP), 114
Rees, M. J. 1984, ARA&A, 22, 471
Reynolds, C. S. 2019, NatAs, 3, 41
Saikia, P., Körding, E., & Falcke, H. 2015, MNRAS, 450, 2317
Seifina, E., Chekhtman, A., & Titarchuk, L. 2018, A&A, 613, 48
Shelton, D. L., Hardcastle, M. J., & Croston, J. H. 2011, MNRAS, 418, 811
Tadhunter, C., Marconi, A., Axon, D., et al. 2003, MNRAS, 342, 861
Tchekhovskoy, A., Narayan, R., & McKinney, J. C. 2010, ApJ, 711, 50
van Velzen, S., & Falcke, H. 2013, A&A, 557, L7
Vasudevan, R. V., Fabian, A. C., Reynolds, C. S., et al. 2016, MNRAS, 458, 2012
Wagner, R. M., Foltz, C. B., Shahbaz, T., et al. 2001, ApJ, 556, 42
Walton, D. J., Nardini, E., Fabian, A. C., Gallo, L. C., & Reis 2013, MNRAS, 428, 2901
Wellman, G. F., Daly, R. A., & Wan, L. 1997a, ApJ, 480, 79
Wellman, G. F., Daly, R. A., & Wan, L. 1997b, ApJ, 480, 96
Xie, F., & Yuan, F. 2017, ApJ, 836, 104
Yuan, F., & Cui, W. 2005, ApJ, 629, 408
Yuan, F., Cui, W., & Narayan, R. 2005, ApJ, 620, 905
Yuan, F., & Narayan, R. 2014, ARA&A, 52, 529